JOHANNES KEPLER
UNIVERSITÄT LINZ | JKU

TNF

Technisch-Naturwissenschaftliche
Fakultät

Charge Modulation Spectroscopy

DIPLOMARBEIT

zur Erlangung des akademischen Grades

Diplomingenieurin

im Diplomstudium

Technische Chemie

Eingereicht von:
Sandra Kogler

Angefertigt am:
Institut für physikalische Chemie

Beurteilung:
o. Univ. Prof. Dr. Serdar N. Sariciftci

Linz, 15. Dezember 2010

Eidesstattliche Erklärung

Ich erkläre an Eides statt, dass ich die vorliegende Diplomarbeit selbstständig und ohne fremde Hilfe verfasst, andere als die angegebenen Quellen und Hilfsmittel nicht benutzt bzw. die wörtlich oder sinngemäß entnommenen Stellen als solche kenntlich gemacht habe.

Linz, am 15. Dezember 2010

Sandra Kogler

Kurzfassung

Charge Modulation Spectroscopy (CMS) ist eine elektro-optische Methode für die *in situ* Untersuchung von strominduzierten Ladungsträgern in organischen Halbleitern, wie rr-P3HT (regioregular - Poly(3-hexylthiophen)).

Die elektro-optischen Eigenschaften eines elektronischen Bauteiles hängen sehr stark von der Art und der Konzentration der Ladungsträger im organischen Halbleiter ab. CMS ist eine wertvolle Methode um diese Eigenschaften zu messen und spannungsinduzierte Ladungsträger und Ladungsträger durch elektrochemische Dotierung zu vergleichen.

Wird durch die angelegte Spannung eine Sperrschicht im Halbleiter erzeugt, geht das CMS Experiment in eine Elektroabsorptionsmessung (EA) über. Aus den Spektren bei unterschiedlichen Spannungen kann durch das EA Signal das im Bauteil bestehende elektrische Feld experimentell bestimmt werden.

Einer der größten Vorteile der CMS Technik ist, dass sie direkt am elektrischen Bauteil, wie zum Beispiel einer Diode oder an einer Metall-Isolator-Halbleiter (MIS) Kombination, durchgeführt werden kann. Die Methode untersucht die Ladungsträger an der Grenzfläche zum Halbleiter und erlaubt so tiefe Einblicke in die elektronische Struktur und Funktionsweise des Bauteiles.

In dieser Arbeit wurden Messungen an Dioden und MIS strukturierten Proben, mit spannungsinduzierten und elektrochemisch zugeführten Ladungsträgern, im sichtbaren und nahen infraroten Bereich des elektromagnetischen Spektrums, durchgeführt.

Zwischen den CMS Spektren der spannungsinduzierten Ladungsträger am P3HT und den durch elektrochemische Dotierung mit Lithiumperchlorat ($LiClO_4$) zugeführten Ladungsträgern sind deutlich Unterschiede erkennbar.

Abstract

Charge modulation spectroscopy (CMS) is an electro-optical method for the *in situ* characterization of injected charge carriers on organic semiconductors, like rr-P3HT (regioregular - poly(3-hexylthiophene)).

The electro-optical properties of devices strongly depend on the kind and the concentration of charge carriers in the organic semiconductor. CMS is an important tool to measure these properties and to compare the results of interfacial doping and electrochemical doping. For the device being biased in full depletion the CMS experiment becomes an electroabsorption (EA) measurement. The built-in field of the device can be obtained by measuring the EA signal at different applied voltages in reverse direction in case of diodes or depletion mode in case of MIS structures.

The main advantage of this measurement technique is that it is performed directly on the electronic device, such as a diode or a MIS (metal-insulator-semiconductor) structured sample. CMS directly probes the charge carriers present at the interface of the semiconductor, allowing a deep insight into the electronic structure and the working principle of the device.

Measurements are performed on both, diodes and metal-insulator semiconductor (MIS) structured samples, using interfacial and electrochemically doped P3HT. The spectral range of the measurement covers the visible and the near infrared part of the electromagnetic spectrum.

In the CMS spectra a difference between interfacial doping of pristine P3HT and electrochemical doping using lithiumperchlorate ($LiClO_4$) in polyethyleneoxide as electrolyte is observed.

Acknowledgment

First of all I want to thank my family for all their support and motivation.

Special thanks go to my mentor Philipp Stadler for his support and advice and Prof. N.S. Sariciftci for giving me the opportunity to work at the internationally noted Linzer Institute of Organic Solar Cells (LIOS).

I also want to thank all the members and visitors of the LIOS institute for their time, help, advice and inspiring discussions, Alberto Montaigne Ramil, Alessandra Operamolla, Almantas Pivirikas, Anita Fuchsbauer, Beatriz Meana- Esteban, Birgit Paulik, Christoph Lungenschmied, Christoph Ulbricht, Cigdem Yumusak, Daniel Egbe, Doris Sinwel, Edina Mujcinovic, Elif Arici-Bogner, Engelbert Portenkirchner, Eric Glowacki, Florian Kuhnlenz, Gebhard Matt, Gerda Kalab, Gülbeden Cakmak, Helmut Neugebauer, Jacek Gasiorowski, Klaus Brandstätter, Mamatimin Abbas, Manfred Lipp, Martin Egginger, Martin Kruijen, Mateusz Bednorz, Matthew White, Mihai Irimia-Vladu, Özlem Usluer, Patchanita Thamyongkit, Petra Neumaier, Robert Koeppe, Sandro Lattante, Serap Günes, Serpil Tekoglu, Stefan Kraner, Stefan Schauer, Stefanie Schlager, Toan Van Pho, Valery Bliznyuk, Yasin Kanbur, Yazmaciyan Aren.

Further I want to thank the members of the SOMAP Institute, Prof. Siegfried Bauer, Alexander Kogler, Joseph Stadlbauer, Melanie Reisinger, Petr Bartu, Reinhard Schwödiauer, Richard Baumgartner and especially Oskar Armbruster for close collaboration and physics lessons.

Contents

Chapter 1

Introduction

1.1 Motivation

Organic materials are used in applications like displays or solar-cells, nevertheless there is still much to be learned about their electronic properties.

The main advantage of organic materials is their solubility in different solvents which keeps the costs of device fabrication low as the semiconducting layer can be applied to the device by spin-coating or inkjet-printing. Those are simple and fast methods, which are also suitable for the realization of low-cost, large area electronic devices on flexible substrates. Another aspect that makes organic semiconductors very attractive for device fabrication is that their properties are very different and can be further tuned by chemical changes of the structure, doping or combination with other materials.

As organic polymeric-semiconductors are used in various devices such as solar-cells or transistors, it is of great importance to understand the nature of charge transport on these polymers and their structural characteristics, in order to optimize the fabrication and the use of these polymers or to synthesize better materials. Determination of structure-property-relationships is rather difficult for semiconducting polymers due to the complexity of being neither fully disordered nor fully crystalline, as for this case proper mathematical models are hard to find.

Up to now the nature of the electronic excitations in conjugated materials remains a topic of lively debate [1]. Measurement methods which are able to probe such excitations will help in this discussion.

An electrical method to detect charge carriers is impedance spectroscopy, which allows to measure the frequency dependence of dielectric effects and charge carriers.

Optical measurements can be highly sensitive to the charge carriers, because polaronic charge carriers show characteristic charge-induced optical absorptions. With charge modulation spec-

troscopy (CMS), it is even possible to obtain spectra of the charge carriers that are located directly at the interface of the semiconductor to the insulator. An advantage of this optical measurement is, that it is performed directly on the device [2],[3].

The nature of the charge carriers on interfacial doped P3HT has been investigated experimentally using CMS technique by different groups [4],[5],[6]. CMS becomes one of the standard techniques for the characterization of semiconducting polymers [7],[8],[9].

The CMS measurements give information about the charge carriers in the semiconductor in different operational regimes. The aim of this work is to use the CMS technique to compare the spectral features of the charge carriers in interfacial and electrochemical doped rr-P3HT (regioregular - poly(3-hexylthiophene), which will be further revered to as P3HT).
We focus on P3HT, because it is an organic semiconductor, which is commonly used in optoelectronical devices. Besides from suitable optical properties the thiophene backbone provides a high stability. As the electroabsorption (EA) method is very similar to the CMS technique, it is also possible to measure the built-in field of a device.

Chapter 2

Theory

2.1 Charge transport in organic semiconductors

2.1.1 Polarons and bipolarons in conducting polymers

In 1973 it was found that the inorganic polymer polysulfur nitride, $(SN)_x$, is a metal [10]. Ever since conducting polymers have been of high scientific interest and they still are. Unlike $(SN)_x$ most other polymeric materials correspond to closed shell systems where all the electrons are paired, such an electronic configuration leads to dielectric polymers.

In 1977 it was discovered that polyacetylene, an intrinsically insulating organic polymer, with an intrinsic conductivity of much lower than $10^{-8}\,\Omega\mathrm{cm}^{-1}$ [11] can be made highly conducting ($10^{3}\,\Omega\mathrm{cm}^{-1}$) by exposure to oxidizing or reducing agents [10]. This process is normally refered to as 'doping' in analogy to the doping of inorganic semiconductors, although the process can be viewed as redox reaction. During 'doping' the neutral polymer is transfered to an ionic complex, consisting of a polymeric cation or anion and a counterion which is in most cases the reduced form of the oxidizing agent, or the oxidized form of the reducing agent. To stay in the terminology of inorganic semiconductors, the use of an oxidizing agent corresponds to p-type doping, while the use of a reducing agent can be viewed as n-type doping. Oxidation or reduction will affect the π-electrons, while electrons of the σ-bond hold the polymer together. The charge can move along the π- conjugated chain [12].

A schematic of an oxidation of a poly(alkylthiophene) chain is shown in figure 2.1, where the introduction of a charge leads to the formation of a polaron.

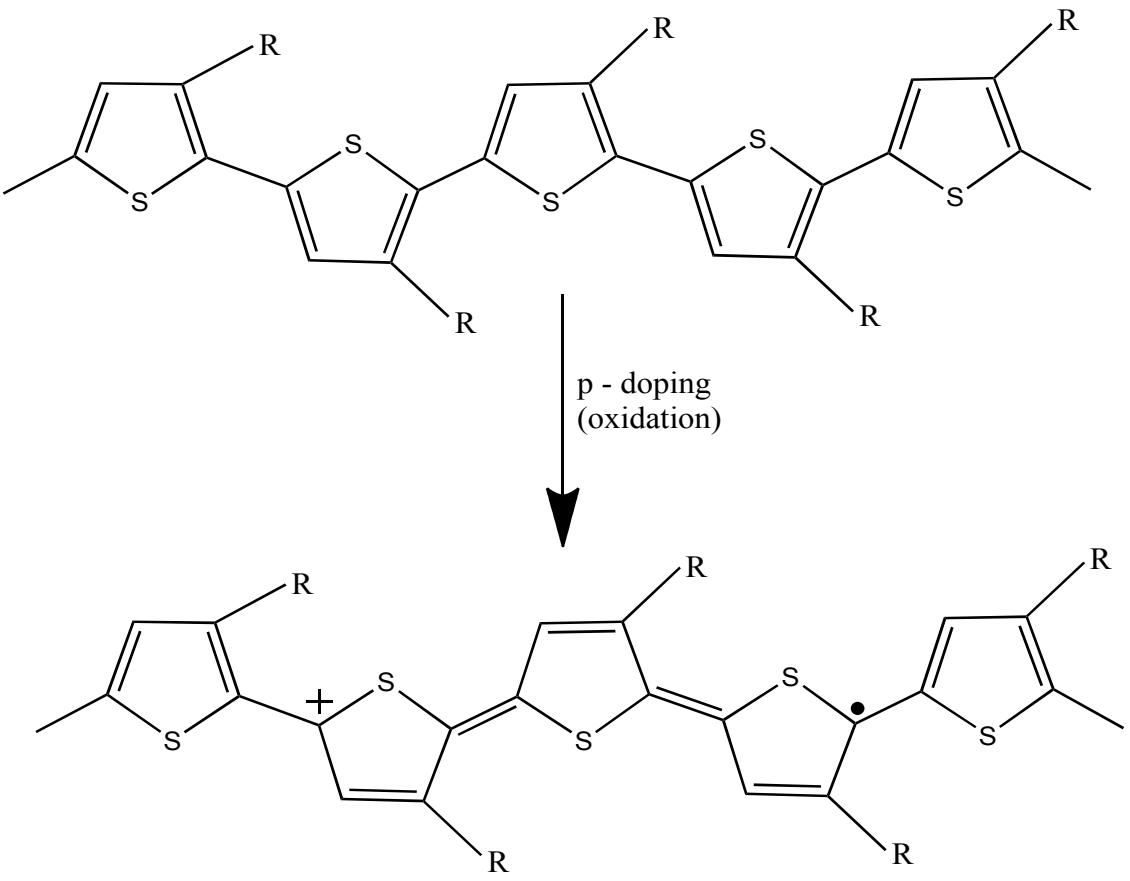

Figure 2.1: Introduction of a polaron onto a neutral poly(alkylthiophene) chain by oxidation (p-doping).

Unlike inorganic semiconductors, conjugated polymers have the ability to change the configuration in the vicinity of charge. In organic polymers the non ionized state does have a different geometry than the ionized state, therefore a distortion in the polymer lattice is produced by the introduction of a charge on the polymer chain. As can be seen in figure 2.1 the charge divides the backbone into areas of different ground states. The ground states of poly(thiophene) are not degenerated, as the quinoid state is of higher energy than the other ground state (figure 2.2). The lattice distortion can be confined to a limited number of monomeric units, therefore polarons are self-localized charged species.

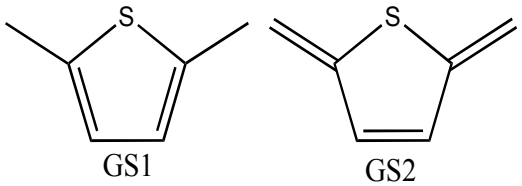

Figure 2.2: Non-degenerate ground states of poly(thiophene).

In case of degenerate ground states, like in *trans* polyacetylene, a charge can move without deformation and dissipation. Therefore it has the properties of a solitary wave and is referred

to as soliton.

An introduction of a charge on a polymer chain leads to change in the energy levels.
In a hypothetical, infinitely straight polymer chain, the highest occupied molecular orbital (HOMO) and the lowest unoccupied molecular orbital (LUMO) states of the neutral polymer chain are fully delocalized along the polymer chain, they show significant dispersion with calculated bandwidths over several electron volts. The highest molecular orbitals (HOMO) contribute to the valence band (VB) and the lowest unoccupied molecular orbitals (LUMO) contribute to the conduction band (CB).

Figure 2.3 (a) shows the energy levels of the neutral thiophene chain [13], the valence and conduction band are indicated. Between the HOMO and the LUMO is a energy gap, which is referred to as band gap E_g in the band model, within the band gap are no allowed states. A transition from the HOMO to the LUMO states is refered to as π-π^* transition.

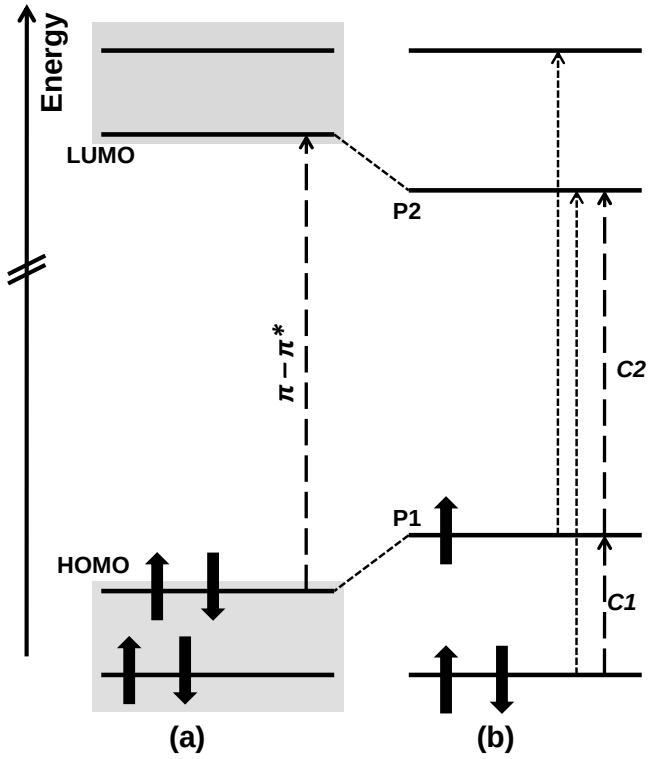

Figure 2.3: Schematic of the energy levels of (a) a neutral polymer chain and (b) a polaron on an isolated chain. Forbidden transitions are indicated (dotted arrows) , but not labeled. HOMO and LUMO describe the highest occupied molecular orbital and the lowest unoccupied molecular orbital.

Figure 2.3 (b) shows that by removing an electron from the highest molecular orbital (HOMO) from a conjugated chain of an organic semiconductor, which is the formation of a positively charged polaron, two new electronic states (polaronic levels, P1 and P2) appear within the π-π^* band gap of the polymer. The parity of these energy states is either *gerade* (even) or *ungerade* (odd). The only allowed transitions are transitions that are accompanied by a change of parity. In the case of an alkythiopene chain carring a polaron, transitions C1 and C2 as shown by slashed arrows in figure 2.3 (b) are allowed, dotted arrows represent forbidden transitions.

The polaronic absorptions are reduced in energy in comparison to the π-π^* absorption of the neutral polymer (figure 2.3 (a)).

In polymeric materials the charge transfer not only happens intramolecular but also intermolecular, the charge carriers have to 'jump' from one polymer chain to another polymer chain. According to H. Sirringhaus polarons in P3HT, a polymer with a high degree of interchain interaction, are not confined to a single chain, but are spread over several, π-stacked chains [14].

For a cofacial dimer the delocalization of the polaron over the two chains leads to a splitting of the polaronic levels into doublets, as shown in figure 2.4 (b). Therefore two new transitions, the charge transfer transitions CT and C3/C3' appear. Symmetry forbidden transitions are not shown in figure 2.4 (b) [5].

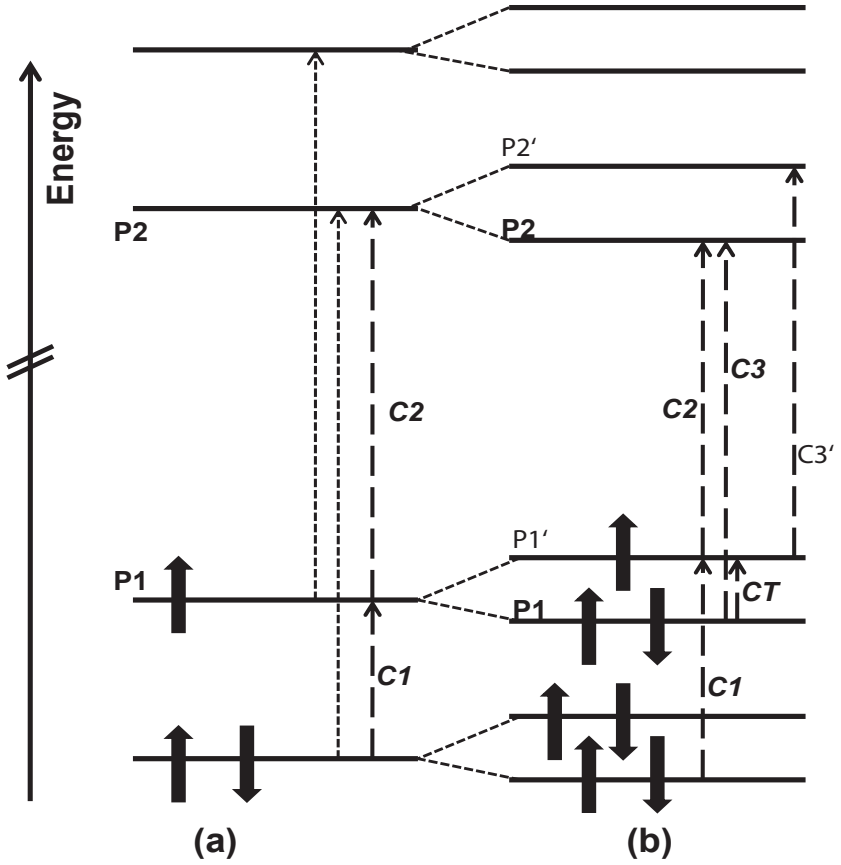

Figure 2.4: Schematic of the energy levels of (a) a polaron on an isolated chain and (b) a polaron delocalized over two cofacial chains. Forbidden transitions are indicated (dotted arrows) , but not labeled.

In polymers with non-degenerate ground states two kinds of charged excitations can be formed by oxidation or reduction: a singly charged, paramagnetic polaron (S = 1/2) or a double charged diamagnetic bipolaron (S = 0) [15]. If two electrons are removed from the neutral polymer, either two polarons or one bipolaron is formed. It is argued that two polarons merge into one bipolaron due to the strong electron-lattice interaction. The bipolaron is a doubly

charged, spinless species. The energy saved by only forming one instead of two deformations of the chain is said to outweigh the increased Coulomb repulsion. R. A. J. Janssen states that semi-empirical calculations predict a transition between a bipolaron and two isolated polarons as a function of chain length [12]. The delocalization of the polarons strongly depends on the degree of structural order within the polymer.

Calculations for the bipolaron lead to the introduction of new states (BP1 and BP2) within the gap, as shown in figure 2.5 (b) . Those states are closer to the middle of the gap than the polaronic-states (P1 and P2) (figure 2.5 (a)). For a bipolaron on a single polymer chain only one absorption, DC1, is expected as the other is symmetrically forbidden.

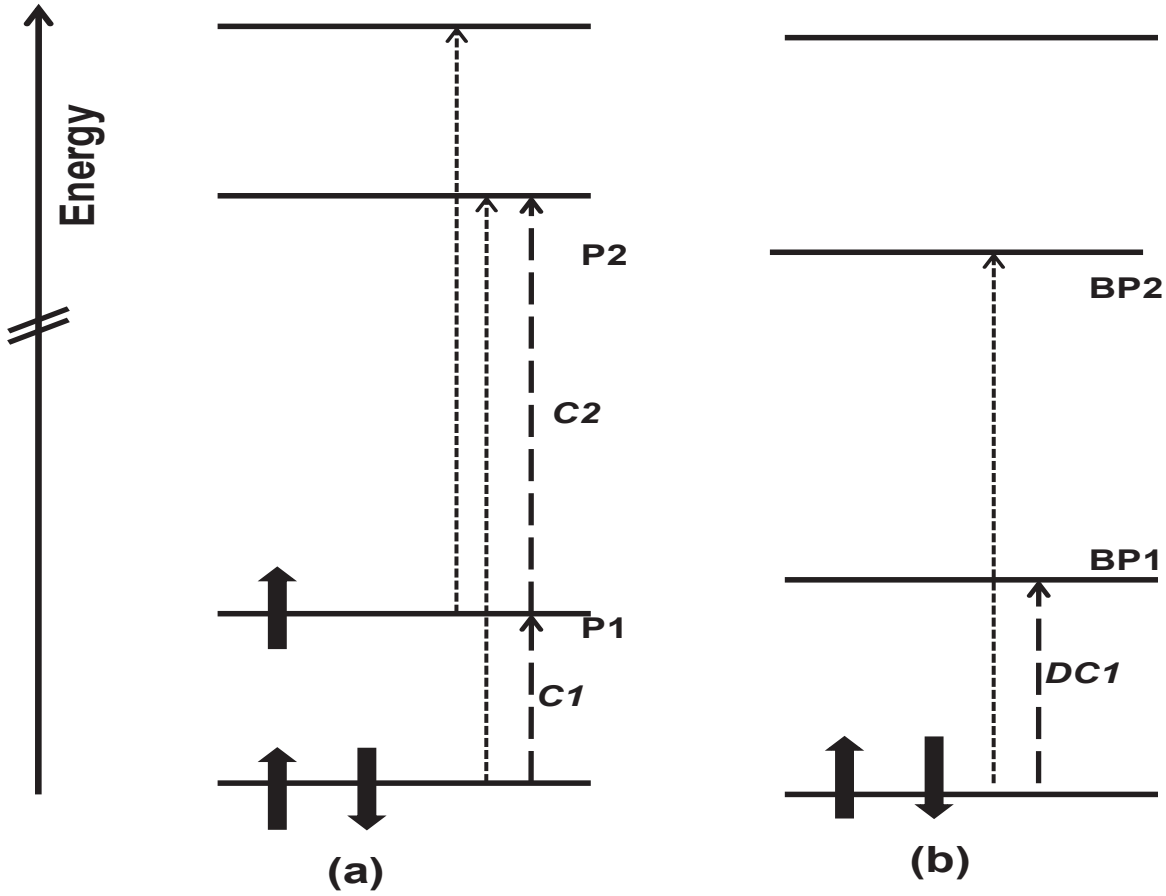

Figure 2.5: Schematic of the energy levels of (a) a polaron on an isolated chain and (b) a bipolaron on an isolated chain. Forbidden transitions are indicated (dotted arrows) , but not labeled.

While the actual absorption spectra of the polaron highly depends on the degree of ordering in the material, the exact molecular structure is less important [16].

2.1.2 Doping mechanisms of organic semiconductors

Organic semiconductors exhibit a negligible intrinsic electrical conductivity due to low charge carrier density and low mobilities [17]. Doping is an tool to increase the conductivity by orders of magnitude [18]. Therein limitations in the performance of organic devices can be overcome. For inorganic semiconductors the concentration of the dopand is low compared to organic semiconductors, where the concentration of the dopand is usually several mol percent. Doping introduces charge carriers onto the semi-conducting polymer, which are delocalized due to the fact that an electron in one repeat unit is attracted to the nuclei in the other repeat units.

Doping of organic polymers can be acomplished in a number of ways, as shown in the schematic 2.6 [19].

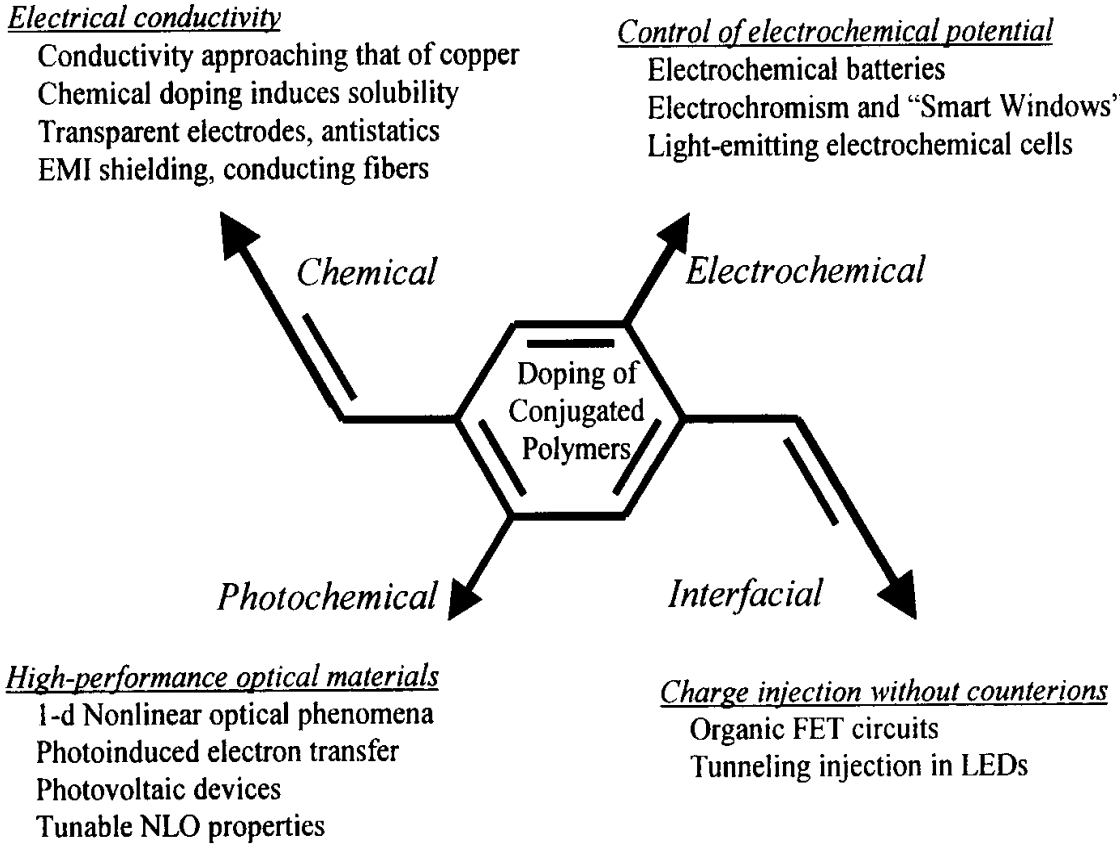

Figure 2.6: Doping mechanisms for organic semiconductors, figure taken from the Nobel Lecture of A.Heeger [19].

chemical doping:
The organic semiconductor is exposed to an oxidizing or reducing agent like iodine or bromine in case of oxidation or alkali metals in case of reduction of the polymer. Oxidation leads to an introduction of positive charges on the polymer chain and is therefore, in analogy to the doping of inorganic semiconductors, referred to as p-doping. A reduction adds a negative charge on the

polymer chain, and is therefore referred to as n-doping. The ions of the reduced oxidizing or the oxidized reducing agent stay in the polymer to compensate the introduced charges. Through the help of chemical doping, organic materials can reach a conductivity which is approaching the conductivity of copper. Further chemical doping induces solubility [19].

- p-doping via oxidation

$$(\pi - polymer)_n + 3/2\, nx(I_2) \rightarrow [(\pi - polymer)^{+x}(I_3^-)_x]_n \tag{2.1}$$

- n-doping via reduction

$$(\pi - polymer)_n + [Na^+(Napthtalide)^-]_x \rightarrow [(Na^+)_x(\pi - polymer)^{-x}]_n + (Naphth)^\circ \tag{2.2}$$

electrochemical doping
Normally electrochemical doping is performed in an electrochemical cell. Usually the working electrode is coated with the organic polymer. The electrode is dipped into an electrolyte solution in which the polymer is insoluble. An electrode supplies the redox charge to the conducting polymer while ions diffuse into (or out of) the polymer from (in) the electrolyte to compensate the electronic charge. By reaching the appropriate voltage between the electrodes in an electrochemical cell the polymer is either oxidized or reduced and counter-ions from the electrolyte solution enter the polymer film in order to balance the introduced charges. The doping level can easily be controlled by actuation of the electrochemical potential.

- p-doping via oxidation

$$(\pi - polymer)_n - x(e^-) + [Li^+(ClO_4^-)] \rightarrow [(\pi - polymer)^{+x}(ClO_4^-)]_n + Li_x^+ \tag{2.3}$$

- n-doping via reduction

$$(\pi - polymer)_n + x(e^-) + [Li^+(ClO_4^-)] \rightarrow [(Li^+)_x(\pi - polymer)^{-x}]_n + (ClO_4^-)_x \tag{2.4}$$

interfacial doping:
Interfacial doping is a charge injection of either holes or electrons at the interface from a metal to the π and π^* bands of an organic semiconductor: [19]

- Hole injection into an filled π-band (p-doping)

$$(\pi - polymer)_n - x(e^-) \rightarrow (\pi - polymer)_n^{+x} \tag{2.5}$$

- electron injection into an empty π^* band (n-doping)

$$(\pi - polymer)_n + x(e^-) \rightarrow (\pi - polymer)_n^{-x} \tag{2.6}$$

A charge injection from the metal to the organic semiconductor causes an oxidation or a reduction of the polymer, as electrons are removed (p-doping) or added (n-doping). In contrast to other doping-mechanisms interfacial doping does not introduce counter ions. The doping lasts only as long as the biasing voltage is applied.

photo doping:
Photodoping is caused by photo-absorption and charge separation, which causes an local oxidation and a nearby reduction. The photo conductivity lasts only until the excitations are either trapped or decay back to the ground state.

$$(\pi - polymer)_n + h\nu \rightarrow [\pi - polymer^{+x} + \pi - polymer^{-x}]_n \tag{2.7}$$

The conductivity introduced on the polymer by chemical doping or electrochemical doping leads to a permanently increased conductivity, while in interfacial and in photodoping the increased conductivity is not permanent.

2.2 P3HT

A polythiophene chain forms the backbone of P3HT. Polythiophene chains are relatively stable in air after $p-$doping. Therefore derivates of polythiophene, like P3HT (figure 2.7) or PEDOT (poly(3,4-ethylenedioxythiophene) are commonly used in optoelectronic devices. The structures of P3AT's (poly(3-alkylthiophene)) have been investigated by Prosa et.al. [20].

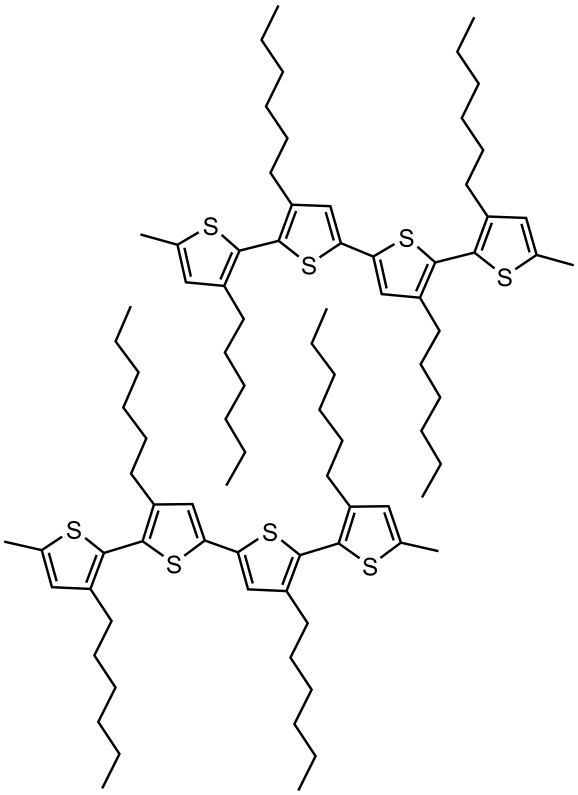

Figure 2.7: Structure of regio-regular head-to-tail coupled poly (3-hexylthiophene).

Polymers with a polythiophene backbone do have nondegenerate ground states as shown in figure 2.2. [21]. As the formation of solitons is only possible in the case of degenerate ground states, on polythiophene either polarons or bipolarons as charged species are formed, same goes for P3HT [22].

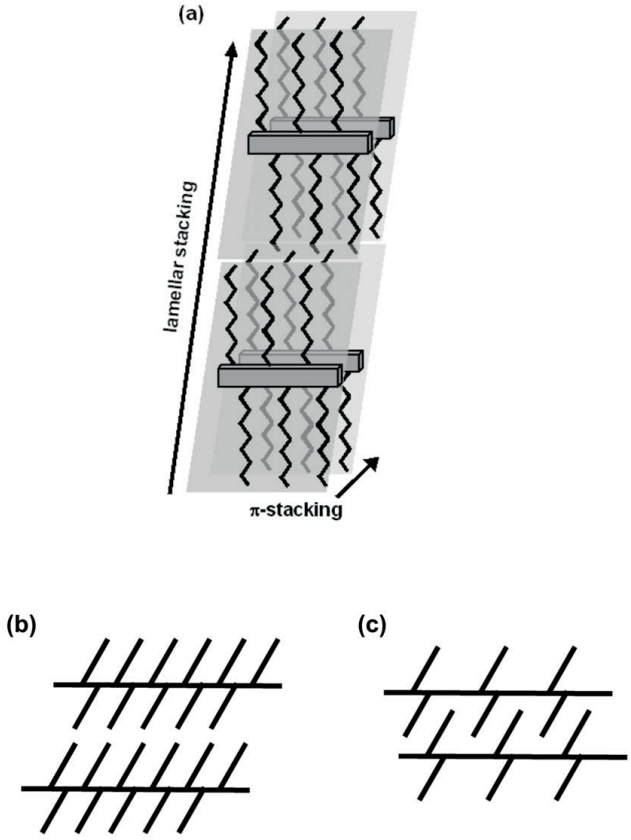

Figure 2.8: (a) Schematic of the packing structure of layered alkylated semiconducting polymers where the side chains cause laminar stacking and the planar backbones lead to π stacking. The side chains may be layered (b) end to end or (c) interdigitated depending upon their attachment density along the backbone or whether they are linear or branched. Figure taken from 'Characterization of semiconducting polymers for thin film transistors', J.Vac.Sci.Technol.B by Michael L.Chabinyc et.al. [7].

In P3HT the conjugation lengths are relatively long, due to a lamellar organisation parallel to the substrate (figure 2.8), which is induced by the hexyl-side chains. The great conjugation length and the π-π stacking, due to the lamellar packing, cause a for organic semiconductors relatively high charge mobility in P3HT. The structure of P3HT is shown in figure 2.7. The preferential orientation of the lamellae is the direction of the π-π stacks in the plane of the film, therefore two dimensional sheets are built by strongly interacting conjugated chains with interchain distance on the order of 3.8 A [5],[7] which allows the charge carriers to delocalize between the chains.
For P3HT the conjugation length is small compared to the device dimensions, therefore the charge transport strongly depends on interchain hopping of the polarons.
P3HT has been intensively investigated, as its regioregular form shows in organic field effect transistor (OFET) applications values of mobility which are comparable to those of α-Silicon 2.6.

Beljonne, Cornil, Sirringhaus and colleagues report that there are differences in the optical absorptions of polarons in the microcrystalline materials, as compared to chemically doped polythiophene in solution. They attribute this differences to the delocalization of polaronic

species over several adjacent polythiophene chains [5].

2.3 Charge modulation spectroscopy

CMS is an experimental technique which is suited for characterizing charged excitations of conjugated doped polymers. Upon the charge injection on organic semiconductors new states within the band gap are formed which can be detected as changes in the optical absorption.

By applying a voltage to a metal-semiconductor-insulator structured sample the concentration of charge carriers at the semiconductor/insulator interface will change.

1. When a negative voltage is applied to the blocking contact (gate) holes gather at the semiconductor - insulator interface. The formation of the accumulation layer is schematically shown in figure 2.9a.
2. A positive bias at the blocking contact increases the depletion layer from the semiconductor - insulator interface into the bulk of the semiconductor. When the entire width of the semiconductor layer is depleted (full depletion) the CMS experiment basically becomes an electro absorption experiment (EA). The formation of the depletion layer is schematically shown in figure 2.9b.

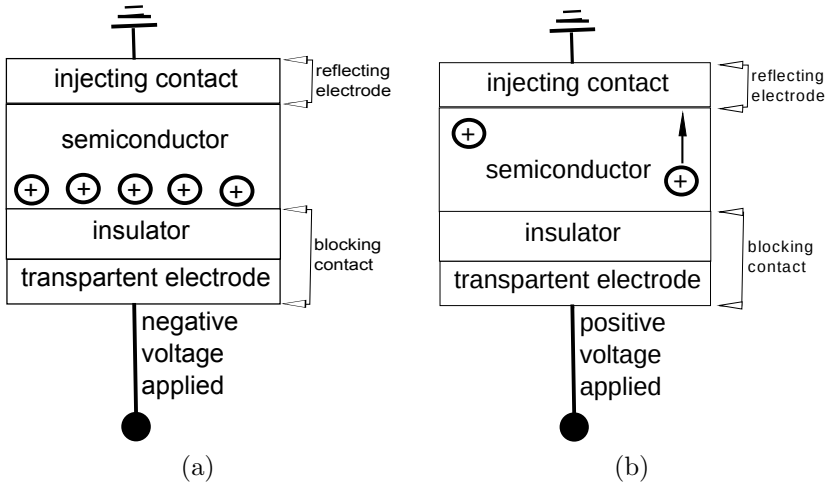

Figure 2.9: (a) Formation of an accumulation layer at the semiconductor - insulator interface and (b) depletion of holes from the semiconductor.

Charges that are trapped at the interfase or that are part of the current flow do not contribute to the oscillator strength of the features in the absorption spectra [23].

In case of double path transmission light passes the transparent electrode and is reflected at the other contact (figure 3.4).

A CMS spectrum plots the change in the optical transmission as a function of the wavelength of the incident light. CMS spectra are taken at various gate voltages.

The changes in the charge carrier concentration at the interface, caused by an AC voltage, are detected using a photo-diode and lock-in technique. The different wavelengths are scanned with a monochromator. Furthermore the lock-in technique gives information about the phase-shift.

Using the ATR-FTIR (attenuated total reflectance - Fourier transform infrared spectroscopy) spectra of the charge carriers in the bulk of the semiconductor are obtained.

2.4 Electroabsorption

Electroabsorption (EA) is the change of the absorption properties of a medium as a response to an external applied electrical field. In a semiconductor the absorption edge is shifted to higher wavelengths, or lower energies [24]. The EA is related to the Stark effect.

In case of an electrical device the built-in potential can be determined experimentally and noninvasive by the electroabsorption experiment, where the change in absorption due to the applied electrical field is measured [25].

The EA and the CMS measurement techniques can be observed using the very same setup. For a device biased into full depletion the spectra are dominated by the electro absorption peak and concomitantely features will disappear. In full depletion mode we focus on the field induced qualitative and quantitative changes in the EA peak. Here the charge concentration is low and therefore the screening of an external applied field is weak. On the contrary CMS measurement examines the charge induced absorptions, which are 180 ° shifted in phase to the EA signal. Therefore the EA and the CMS features have a different sign in the spectra when the in-phase signal against the energy is plotted. The CMS signal increases with the carrier concentration during accumulating charges in the device.

2.4.1 Stark-effect

The dipoles in a material will interact with an external applied electric field. As a dipole moment can have two stationary positions in a homogeneous electric field - in direction of the field or opposite - every energy level prior to applying the electric field, will be split in two energy levels symmetric around the field-free level. The energy will depend on the orientation of the dipole within the field. The potential energy will be higher in the case of the dipole moment pointing in direction of the field and lower if it points in the opposite direction.

The splitting of the energy levels, as shown in figure 2.10, under an electric field is described by the Stark effect. The level lower in energy represents the position opposite to the electric

field, while the higher energy level represents the position in direction of the electric field.

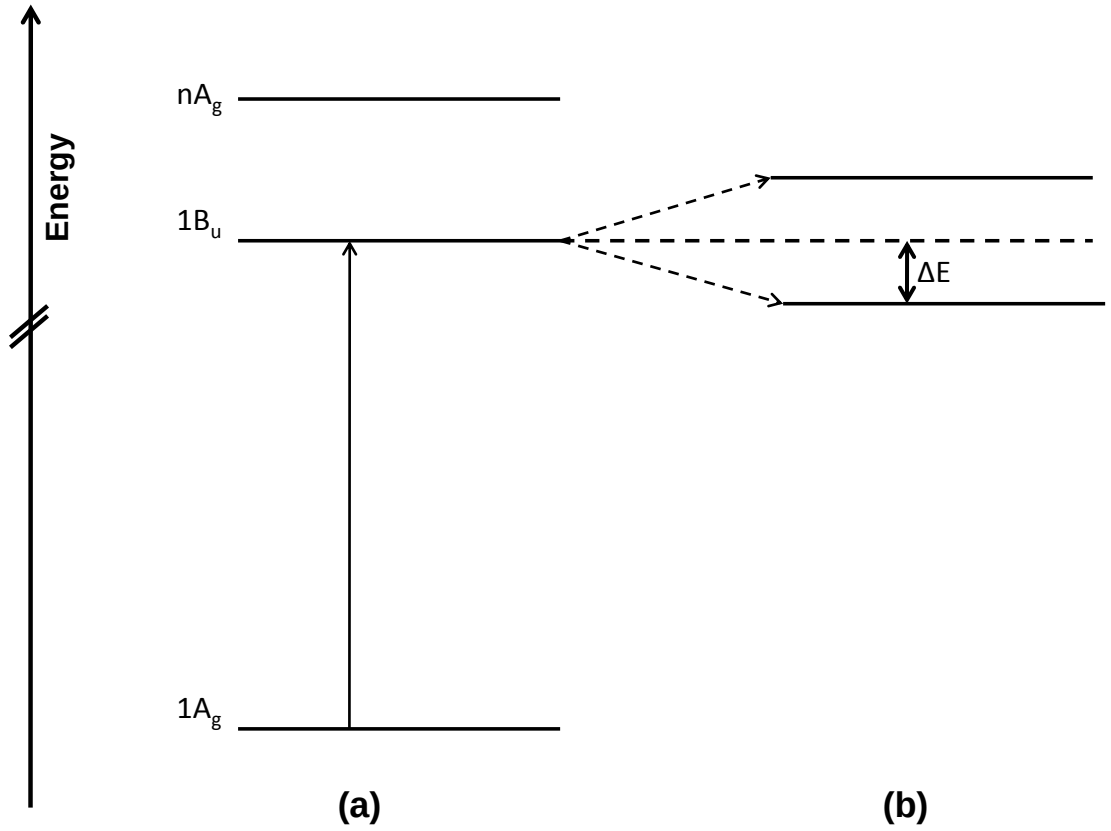

Figure 2.10: Energy levels affected by the Stark Effect; (a)field-free case, (b) energy level-split due to an electric field.

The more probable $1A_g \rightarrow 1B_u$ transition is red shifted, this is called the excitonic Stark shift (ΔE). The applied electric field can also couple the $1A_g$ level to a higher lying state of even parity. Transitions between even parity are usually forbidden, but they become allowed in the presence of an electric field.

The excitonic Stark shift is given as:

$$\Delta E \quad = \quad \vec{\mu}\, F + \frac{1}{2}\, \Delta\vec{p}\, F^2 \tag{2.8}$$

where E represents the photon energy F stands for an externally applied field, $\Delta\vec{p}$ is a second order tensor for the polarizability of the medium and $\vec{\mu}$ is the permanent dipole moment. The first part of the equation which shows a linear dependence describes the interaction in the

presence of permanent dipoles, while the quadratic part describes the interaction of induced dipoles with an external electric field [26].

The Lambert-Beer's law gives the absorption of light by a material,

$$I = I_0\, e^{-\alpha d} \tag{2.9}$$

where I is the intensity of the light, I_0 is the intensity of the incident light. The Transmittance T is defined as:

$$T = \frac{I}{I_0} \tag{2.10}$$

α is the absorption coefficient and d is the thickness of the thin film. The field induced change of the absorption coefficient $\Delta\alpha(E)$ can be described as the difference between the absorption in the presence of an electric field α^F and the unperturbed absorption α. ΔI is the field induced change in the absorption intensity [27].

$$\Delta\alpha(E) = \alpha^F(E) - \alpha = -\frac{1}{d}\, ln(\frac{\Delta I}{I_0}) \tag{2.11}$$

The change in the absorption constant ($\Delta\alpha(E)$) for reflection geometry (double path transmission) is therefore given by

$$\Delta\alpha(E) = -\frac{1}{2d}\, ln\frac{\Delta I}{I_0} \tag{2.12}$$

From the dependence of χ (susceptibility) upon the applied electric field it can be derived that the change in the transmittance $T = \frac{\Delta I}{I_0}$ is proportional to the actual electric field, which is given by the photon energy (E) dependent imaginary part of the third order non-linear susceptibility $Im\chi^{(3)}(E)$.

$$\frac{\Delta I}{I_0} \sim Im\chi^{(3)}(E)F^2 \tag{2.13}$$

If an AC coupled DC voltage is applied to a semiconductor film, the electric field within the film (V_{int}) can be described by

$$V = V_0 + V_{AC}\sin(\omega t) \qquad \text{with} \qquad V_0 = V_{DC} - V_{int} \tag{2.14}$$

Where ω is the frequency of the AC voltage and t is time. The combination of equation 2.14 with equation 2.13 yields

$$\frac{\Delta I}{I} \sim Im\chi^{(3)}(E)\ (V_0 + V_{AC}\sin(\omega t))^2 \tag{2.15}$$
$$\frac{\Delta I}{I} \sim Im\chi^{(3)}(E)\ ((V_{DC} - V_{int}) + V_{AC}\sin(\omega t))^2 \tag{2.16}$$
$$\frac{\Delta I}{I} \sim Im\chi^{(3)}(E)\ (\frac{1}{2}V_{AC}^2\ (1 - \cos(2\omega t))\ +\ 2V_0\ V_{AC}\ \sin(\omega t)\ +\ V_0^2) \tag{2.17}$$

Equation 2.17 can be seperated into two parts, where one is dependent on the first harmonic (1ω) while the other part is dependent on the second harmonic (2ω)

$$\frac{\Delta I}{I}(\omega) \sim (V_{DC} - V_{int})\ V_{AC}\ \sin(\omega t) \tag{2.18}$$
$$\frac{\Delta I}{I}(\omega) \sim V_{AC}^2\ \cos(2\omega t) \tag{2.19}$$

The first harmonic (1ω) response is proportional to the product of the electric field V_0 and the AC amplitude, the second harmonic signal (2ω) depends upon the square of the AC amplitude.

In the case that the applied external field (V_{DC}) compensates the internal electric field (V_{int}) the term ($V_{DC} - V_{int}$), from equation 2.18, becomes zero and the EA response vanishes. Experimentally this can be probed by changing the applied DC bias but keeping the AC component constant.

Chapter 3

Experimental

3.1 Device preparation

3.1.1 Substrate preparation

ITO substrates
For the devices with an ITO (indium-tin-oxide) electrode a $15x15$ mm piece from a glass coated with ITO (15 Ω/□) bought from Kintech Hong Kong is cut. From the edge of the substrates $5x15\,\mathrm{mm}^2$ ITO is etched of with a mixture of $HCl_{(conc.)}$: $HNO_{3(conc.)}$: $H_2O_{(deionized)}$ = 4.6 : 0.4 : 5 . An insulating tape protected the rest of the ITO during the 20 min in an ultrasonic bath. After the etching step the solution was rinsed off by 18.2 MΩ H_2O. Then the samples were cleaned in an ultrasonic bath for 20 min using 2% Hellmanex cleaning solution. The Hellmanex solution was removed by flushing the samples with 18.2 MΩ H_2O. ITO glasses were dried using nitrogen gas.

The ITO is highly reflective in the infrared, nevertheless ITO electrodes can be used down to 0.8 eV as the loss of light intensity in the double path transmission is only around 25 %.

Glass substrates
The glass substrates were cleaned in an ultrasonic bath using a 300 ml H_2O + 5 ml $NH_{3(conc.)}$ solution for 15 min at 80 °C, then 2 ml H_2O_2 (30%) were added and the glasses were left for 15 min more in the ultrasonic bath at 80 °C. Then they were rinsed with 18.3 MΩ H_2O. Glasses were dried using nitrogen gas.

3.1.2 Materials

3.1.2.1 Regioregular Poly(3-hexylthiophene) (P3HT)

Films of P3HT were prepared by spin coating warm solutions of P3HT in chlorobenzene. The solutions had a concentration of either 1 or 3 weight-%. For the spin coating process a program was used, where the sample holder is accelerated for 40 s to 1500 rpm then the sample holder is further accelerated to rotate with 2000 rpm for 20 s. In order to gain thicker films of P3HT also another program for the spin coater was used, were the spin coater in a first step is only accelerated to 800 rpm for 40 s and then for 20 s it is accelerated to 1500 rpm.

The films were annealed for 30 min at 150 °C under nitrogen atmosphere. The annealing process causes a reduction of the free volume in the P3HT layer and a removal of the residual solvent, thus leading to more compact and ordered films.

3.1.2.2 Benzocyclobutene derivative (BCB)

Divinyltetramethyldisiloxane-bis(benzo-cyclobutene) (BCB) (figure 3.1) polymerizes thermally in a cycloaddition reaction, thus no side products are released. To get a fully crosslinked BCB the samples were heated to 250 °C under nitrogen atmosphere (in order to avoid oxidation). BCB shows a permitivity ϵ of typically 2.6 to 2.8 [28] and a geometric capacitance C_D of 1.8 nF cm^{-2} measured for a 14 mm^2 and 1 μm device.

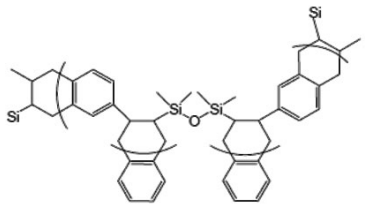

Figure 3.1: Structure of BCB.

BCB is used as an insulator in the MIS samples. Films were prepared by spin coating the Cyclotene solution by Advanced electronics resins. For the spin coating process a program was used, where the sample holder is accelerated for 40 s to 1500 rpm and kept at that velocity for 40 s then the sample holder is further accelerated to rotate with 2000 rpm for 20 s. After spin-coating the samples were heated to 250 °C under nitrogen over night.

Benzocyclobutene (BCB) acts as a trapping-free dielectric, because it is free of charge trapping groups that can have a large electron affinity [14],[28].

3.1.2.3 Poly(ethyleneoxide) (PEO)

Acetonitrile is used as a solvent for the PEO with a molecular weight of 100000 g mol^{-1}, bought from Aldrich. The solution is spin-coated using the same program for the spin coater as for the BCB films. Then the films are heated to 45 °C for 30 min under nitrogen atmosphere. The PEO together with the $LiClO_4$ serves as electrolyte layer, which is used to show the effect of doping on the CMS measurements.

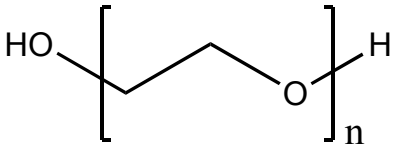

Figure 3.2: Structure of PEO.

3.1.2.4 Lithiumperchlorate ($LiClO_4$)

$LiClO_4$ provided by Alfa Aesar is used as an ionic component in the PEO films. It is commonly used as solid-gel electrolyte in lithium batteries.

3.1.3 Evaporation of the electrodes and installation

The metal electrodes were applied by thermal deposition through a shadow mask at a pressure of approximately 10^{-6} mbar, using tungsten boats as a source. For the reflecting electrodes a film thickness of at least 100 nm was vapor deposited to ensure a good reflection.
As contacts gold, aluminium and samarium were utilized. For measurement the devices were mounted in the cryostat within the glove box, a small droplet of silver paste was used to gain a good contact. The P3HT films were spin coated in air, afterwards the films were annealed under nitrogen atmosphere. A slight doping of the P3HT from the residual oxygen can not be excluded.
The cryostat was evacuated to pressures lower than 10^{-5} mbar.

3.2 Experimental setup and measurement technique

3.2.1 CMS using a lock-in technique

Figure 3.3 schematically shows the measurement setup used for the CMS and EA measurements.

Disperse light from a lamp passes a filter, which is installed to prevent light from higher orders of refraction to pass the monochromator. In the monochromator, due to a mirror system, only the desired wavelength can pass the exit slit. A mirror and lens system focuses the light beam at the desired spot of the sample, which is mounted in a cryostat. The sample in the cryostat can be cooled to liquid nitrogen temperature. The light beam is reflected at the back of the sample, therefore the light passes the sample twice (double path transmission), as shown schematically in figure 3.4. Depending upon the different layers in the sample several reflections can occur, which is schematically shown for a MIS in figure 3.4.

Field independent reflections do not influence the observed spectra as due to the lock-in technique only the field dependent changes in the transmitted light are detected. Lenses guide the reflected light to the detector, which passes a signal to the lock-in amplifier.
In case of a background measurement (T) no bias is applied to the sample. The lock-in amplifier is referred to the chopper frequency. The background spectra are recorded using the lock-in technique so that they are comparable to the derivative spectra (δT) , where the lock-in amplifier is referred to the frequency of an AC coupled DC signal that is applied to the sample. A computer controls the function generator and the monochromator and reads out the measurement data from the lock-in.

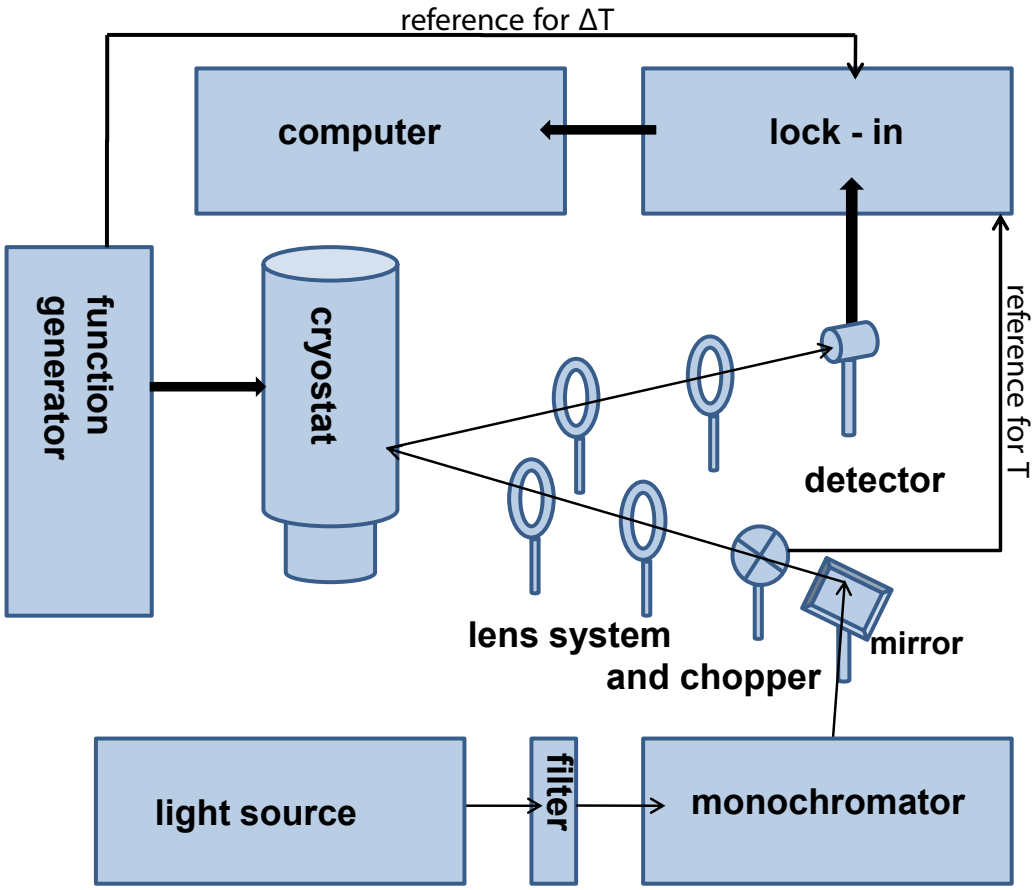

Figure 3.3: Schematic of the measurement setup used for the CMS and EA measurements.

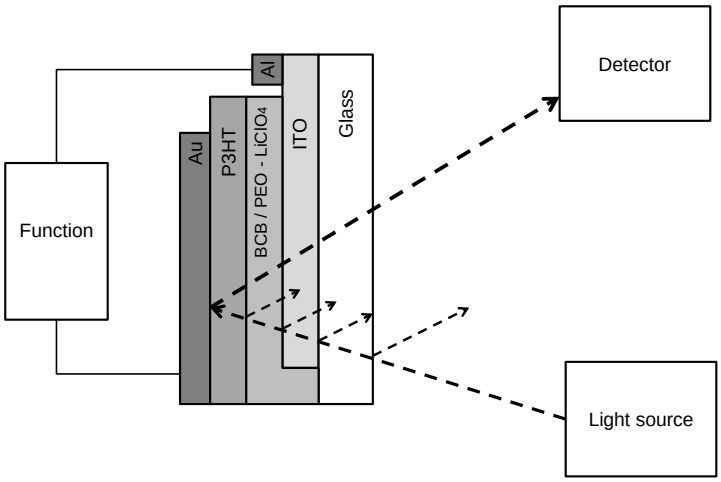

Figure 3.4: Schematic picture of the possible reflections of the light beam within a MIS-structured sample.

For the CMS spectrum firstly a background (T) with no voltage being applied to the sample is measured. The lock-in amplifier uses the chopper frequency to detect the signal. Then an AC coupled DC voltage varies the amount of charge carriers in the semiconductor, with the amplitude of the AC being small compared to the DC voltage, giving the (δT) spectrum, where the lock-in is locked onto the frequency of the AC bias.

The spectra of (δT) are normalized by a division through the background scan (T), $\frac{-\delta T}{T}$, in order to get rid of the spectral response due to the characteristics of the setup. These characteristics include the intensity distribution of the lamp, the performance of the monochromator and the sensitivity of the detector.

For the measurement in the visible and the near-infrared part of the electromagnetic spectrum of light two different light sources were used. For the visible part of the electromagnetic spectrum a xenon-short-arc-lamp XBO 150W/1 lamp was utilized, while for measurements in the infrared a Philips Infrared lamp BRI25 IR Red 150W 230-250V E27ES was installed. The arc lamp is mounted in a lamp housing LAX 1530 by Müller Optic-Electronics, which cools the lamp and focuses the light beam. For the Philips IR lamp a condensor lens of 7.5 mm diameter focuses the light, and a fan (dismounted from an old computer) cools the lamp.
A filter wheel by Acton Research Cooperation containing filters for different wavelengths cuts out lower wavelengths of the spectra before the light enters the monochromator and therein prevents the measurement of peaks which are due to a higher order of refraction.
The grating, Acton Spectra Pro 150, contains of different grid sets, of which two with BLZ = 800 nm and BLZ = 2 μm were used. The opening of the entrance and exit slit, each 1.15 mm, is a compromise of delivering sufficient light and having a good spectral solution.
Different optical lenses and a mirror guide the light to the sample, and the reflection to the detector.
For the measurement of the background spectra the lock-in amplifier is locked onto the frequency

of a chopper wheel by Scitec instruments.
The sample was mounted in a cryostat, 'Optistat DN-V' by Oxford Instruments which was evacuatedby a Pfeifer Vacuum Turbo Cube, DCU. The measurements were performed at room temperature (RT, 275 K).
A function generator (Stanford Research Systems, Model: DS345) applies the bias to the sample. For samples with a dielectric layer of BCB a high-voltage amplifier by Trek (Model 610D, COR-A-TROL) enhanced the bias.
For the detection a Si-detector was used to cover the visible part of the spectra, while for the infrared part an InGaAs-detector was used.
An amplifier (FEMTO, DLPCA-200) changed the current to an amplified voltage signal, before passing it on to the lock-in.
A less noisy signal is obtained if every single part of the setup is connected star-like to a common ground.
The computer reads out the measurement output from the lock-in (Stanford Research Systems SR 830) using a GPIB interface.
We designed a computer program to control the setup, which allows to set an *AC* and/or *DC* voltage sequence and to change the wavelength. The program reads out the spectra with the lock-in either referenced at the *AC* signal or the frequency of the copper wheel.
The light-path is protected from ambient light by a box, which is coated with black optical foil on the inside to prevent unwanted reflections, and aluminium foil from the outside. Ambient light, even if not modulated with the reference frequency, will cause an increase in the noise, therefore it is of benefit to keep the ambient light out. Before the actual CMS measurements, with the samples mounted in the cryostat and under vacuum, current-voltage (IV) curves were recorded using a Keithley Instruments 2400 Source Meter.

An oscilloscope was used to probe the electrical signals, which was of great help, especially in the boarders of functionality of the instruments.

For the first tests of the setup different diodes were measured in order to compare the spectra to those in the diploma thesis of C.Lungenschmied [25]. After some optimization steps MIS structured samples were measured, which base upon the same principle as the FET (field effect transistor).

The final configuration of the setup is now highly optimized, so that even the very weak CMS signal is easily detected, containing only a small amount of noise. Also the sample build-up and geometry were optimized to lead to good results. Samples with big electrodes have the advantage that the light beam can easier be focused, therefore big electrodes lead to a higher amplitude of the signal. The setup is highly flexible, with small changes different but surely interesting measurements could be made.

3.2.2 CMS using a ATR - FTIR technique

3.2.2.1 Michelson interferometer

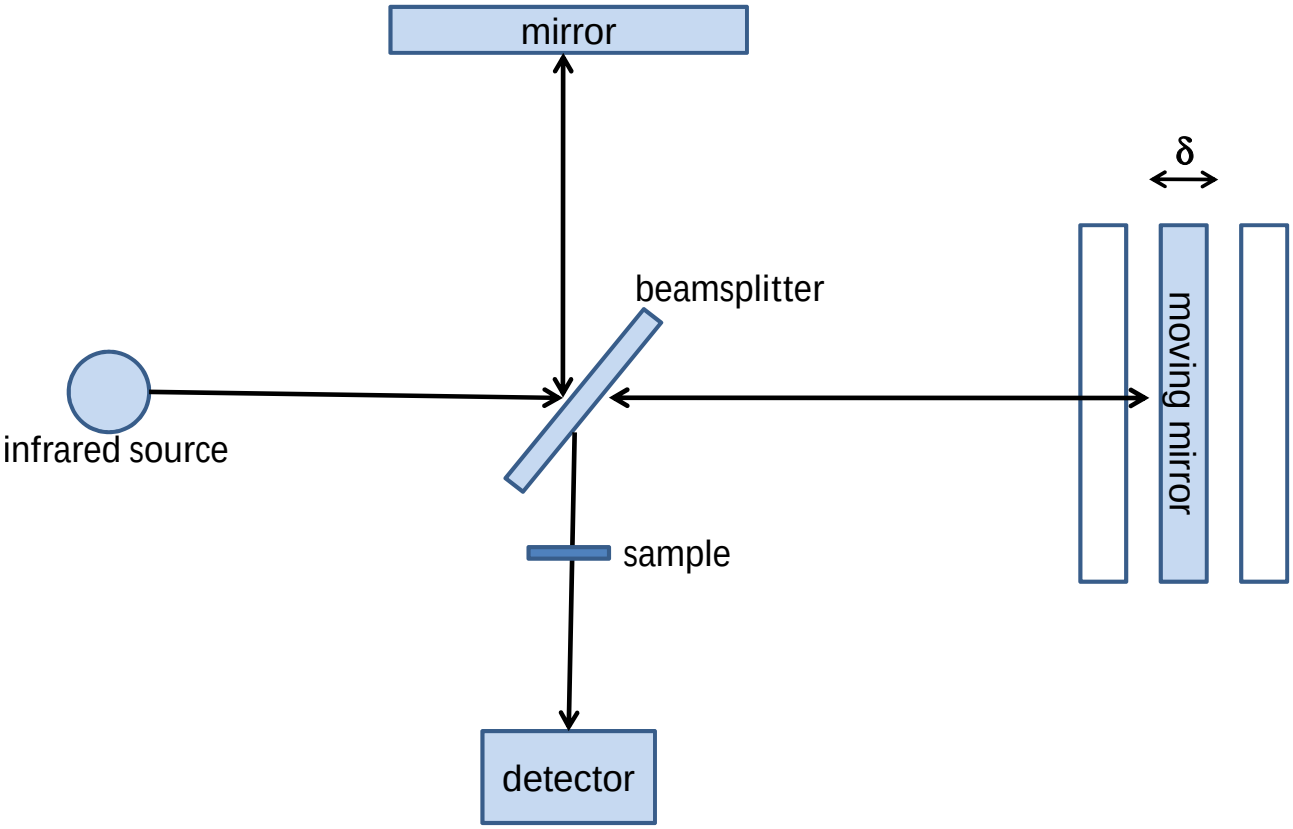

Figure 3.5: Schematic of a Michelson interferometer

Figure 3.5 shows schematically the principal of a Michelson Interferometer.

Light from a broadband infrared source is splitted at a beamsplitter. 50% of the light is transmitted to a fixed mirror, while the other 50% are reflected to a moving mirror. The reflected light passes the beam splitter again and recombines at the other side of the beamsplitter. Due to the moving mirror the light has traveled different distances which leads to an interference. The path difference of the light due to the motion of the mirror is called *optical path difference* (OPD) or *optical retardation* δ. The light then passes through the sample before entering the detector.

The plot of the intensity variation of light as a function of optical retardation (the intensity registered at the detector as a function of the moving mirror position), is known as the *interferogram* $I(\delta)$. At zero path difference (ZPD) position, when the two mirrors are equidistant from the beamsplitter all wavelengths of light will interfere constructively. In the other cases some wavelengths will interfere constructively while others will interfere destructively.

In addition to the light from the infrared lamp light from a Helium-Neon (HeNe) laser passes the optical path. Because the laser light is monochromatic it creates a sine-squared interferogram pattern behind the beamsplitter. The interferogram of the HeNe laser helps to detect the exact mirror position during the FTIR scan.

The data obtained from a Michelson interferometer is light intensity versus mirror position, only through a mathematical calculation the spectra, transmittance T as a function of the wavelength, are obtained. This mathematical calculation is called Fourier Transformation (FT).

For a transmission experiment, first a interferogram without the sample being present is measured, which when Fourier transformed yields the *background* or T_0 spectrum. Then the interferogram with the sample is measured, which when Fourier transformed yields the T spectrum. These two spectra can be used to either calculate the transmittance $[T/T_0]$ or the absorbance spectrum of the sample.

3.2.2.2 ATR-FTIR technique

A schematic of the ATR-FTIR samples is shown in figure 3.6. The ATR crystal acts as a reflection element and waveguide for the infrared light beam and as an electrode for the sample. Within the ATR crystal the light beam is reflected several times, the evanescent wave interacts with substances near the surface where it is partly absorbed. Therefore it has to be conductive, chemically and electrochemically stable, transparent in the infrared spectral region and it must have a high refractive index [29]. Only a few materials fulfill those demands like slightly p-doped silicon or slightly n-doped germanium.

In our work we used silicon ATR crystals, as silicon has an appropriate transparency in our measurement region. The penetration depth is calculated to be $100 - 150\,\mathrm{nm}$. The refractive index of silicon is $\epsilon = 3.4$, while the refractive index of the majority of organic samples is in the area of $\epsilon = 1.5$ [30]

In order to prevent pinch-troughs when applying the contact to the gold electrode we put a droplet of a 7 % PMMA solution on top. We applied the silver paste on the droplet in a way that at the edge of the PMMA it would be in contact with the gold electrode. Then we connected the wire to the silver paste atop of the PMMA film, this is schematically shown in figure 3.6.

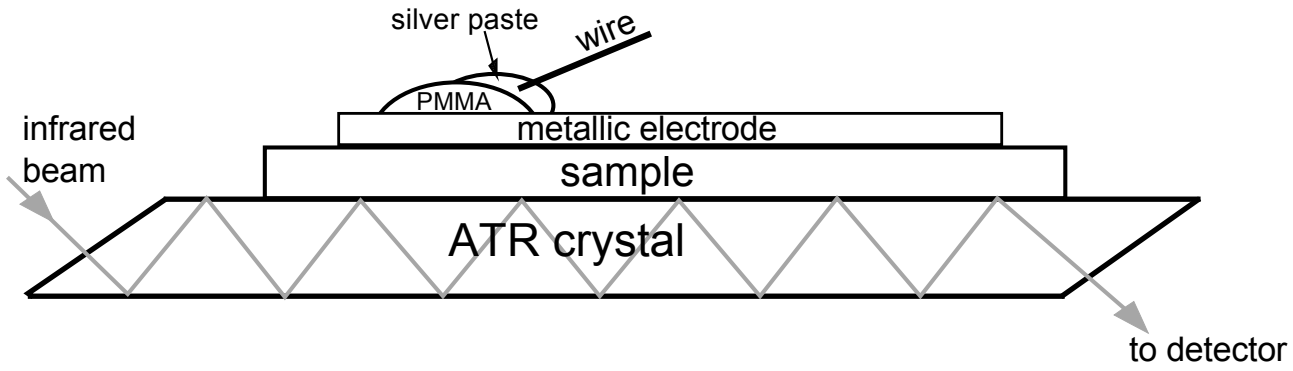

Figure 3.6: Schematic of Silicon ATR crystal used in this work. Arrows indicate the IR light beam. The metallic electrode is necessary to apply a voltage on the film.

Spectra are measured with (T_{ON}) and without (T_{OFF}) an applied DC bias, from which the differential spectra are then calculated (equation 3.1).

$$\frac{-\Delta T}{T} = \frac{-(T_{ON} - T_{OFF})}{T_{OFF}} \tag{3.1}$$

For the applied bias being on (ON-state) or off (OFF-state) 10 spectra are measured, this scans are repeated 1200 times.

For the infrared measurements we used a Bruker IFS 66/S FTIR spectrometer. The spectrometer is equipped with a KBr (potassiumbromide) beamsplitter, an InGaAs (indium-gallium-arsenide) detector and a MCT (mercury-cadmium-telluride) detector. Before starting the measurements the sample chamber is purged with nitrogen for at least 60 min. A software controls the scan parameters and triggers the applied voltage.

To compare the influence of ions on the FTIR spectra, either P3HT (figure 3.7a) or P3HT + PEO + $LiClO_4$ (figure 3.8a) were spincoated on the crystal.

The silicon is covered with a thin layer of natural oxide. Therefore in case of the ATR sample with a P3HT layer a MIS like behavior is observed, if a voltage is applied (figure 3.7b and 3.7c).

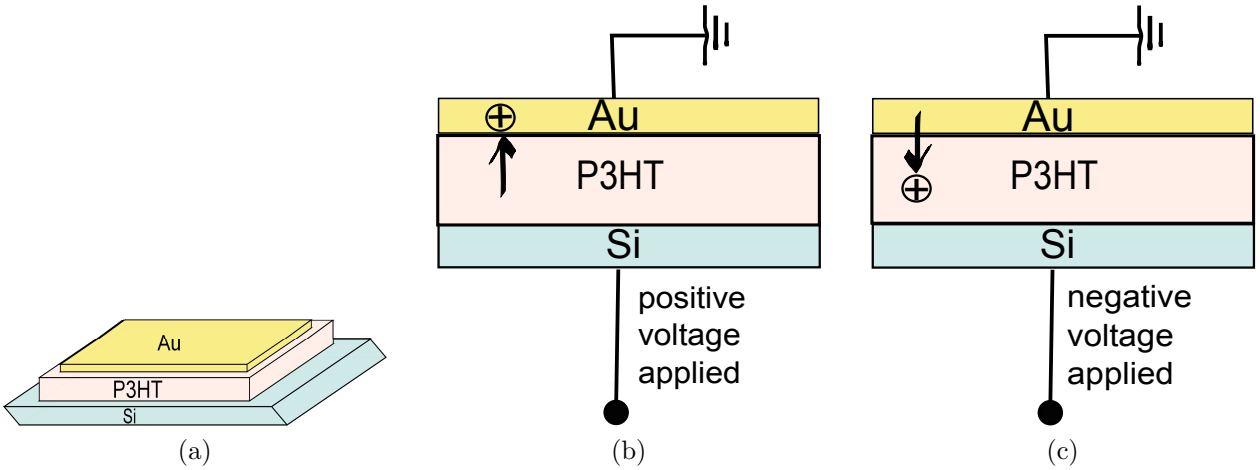

Figure 3.7: (a) Schematic of the ATR sample (b) positive voltage applied to the silicon crystal (c) negative voltage applied to the silicon crystal

In case of the additional layer the sample is basically an electrochemical cell, where the PEO + $LiClO_4$ acts as a solid electrolyte (figure 3.8a). If a positive voltage is applied to the silicon, the P3HT is p-doped, ClO_4^- counterions diffuse into the semiconducting layer (figure 3.8b). While if a negative voltage is applied, the P3HT is n-doped and Li^+ ions diffuse into the layer (figure 3.8c).

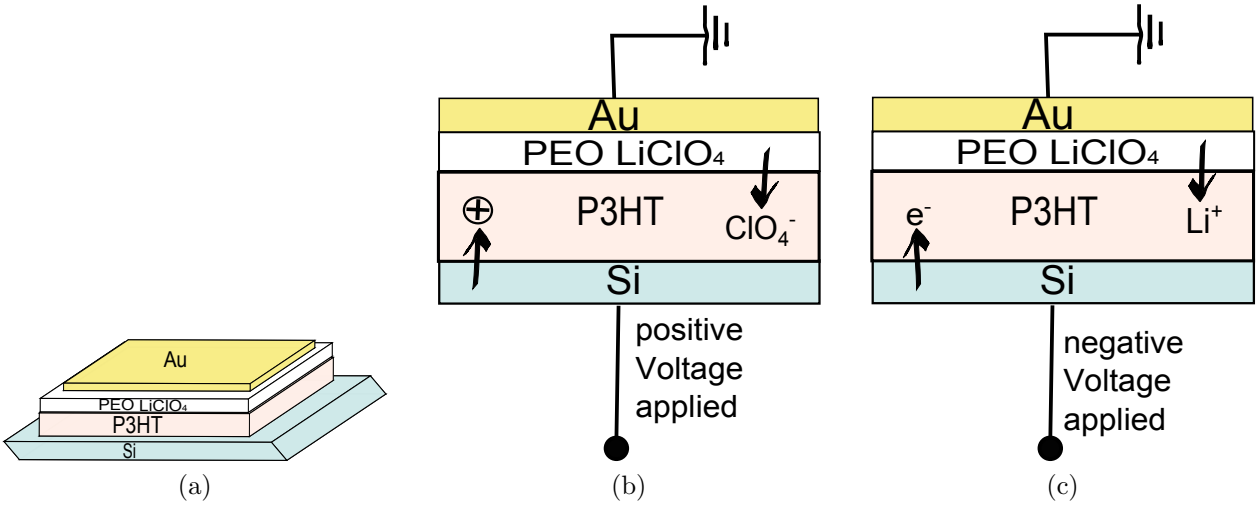

Figure 3.8: (a) Schematic of the ATR sample (b) positive voltage applied to the silicon crystal (c) negative voltage applied to the silicon crystal

After spincoating the P3HT layers had a thickness of 220 nm, the ion containing PEO layers had a thickness of $50 - 70$ nm.

3.2.3 Comparison lock-in and ATR-FTIR technique for CMS

The lock-in technique is used for measurements in the visible and the near infrared part of the electromagnetic spectrum. For the middle infrared another detector and other lenses would be needed, therefore we decided to cover this part of the spectrum using the FTIR technique.

For the visible and the near infrared the devices are built on substrates of glass, for the middle infrared ATR-crystals of slightly p-doped silicon is used.

Using the ATR-FTIR method for the CMS measurements has some advantages compared to the scanning IR measurement: [31]

- The FTIR method is much less time-consuming than a standard IR measurement, because all wavelengths are measured at once.
- The FTIR method shows a better signal-to-noise ratio as the light intensity on the sample is much higher than during a scanning measurement.
- The exact position of the mirror is measured with the aid of a laser signal. Therefore the spectra can be calculated with a high precision to the wavenumbers.

Also there are disadvantages of the FTIR measurement:

- The FTIR method does not give information about the phase.
- Difference spectra are calculated from measurements with applied bias and those without. If no bias is applied the intrinsic charge carriers are probed. For a DC being applied the charge carriers for that voltage are probed. The difference therefore gives information about the charge carriers at the interface and in the bulk present at the applied bias minus the intrinsic carriers. In the lock-in technique the applied AC bias will change the charge carrier concentration at the interface, while the bulk concentration stays the same due to the applied DC bias. Therefore the lock-in technique will give information about the charge carriers located at the interface.

It has to be mentioned that the ATR-FTIR gives difference spectra ($\frac{-\Delta T}{T}$) , while the lock-in technique gives derivative spectra ($\frac{-\delta T}{T}$) as the lock-in only measures the changes in the detected signal.

Chapter 4

Results and discussion

4.1 P3HT absorption spectra

Before coming to charge modulation spectroscopy the optical absorption of P3HT was measured in the setup as described before. The absorption edge of P3HT is observed around 1.85 eV (figure 4.1b), the increase in absorption at low energies (figure 4.1a) is mainly attributed to the reflectance of ITO in the near infrared.

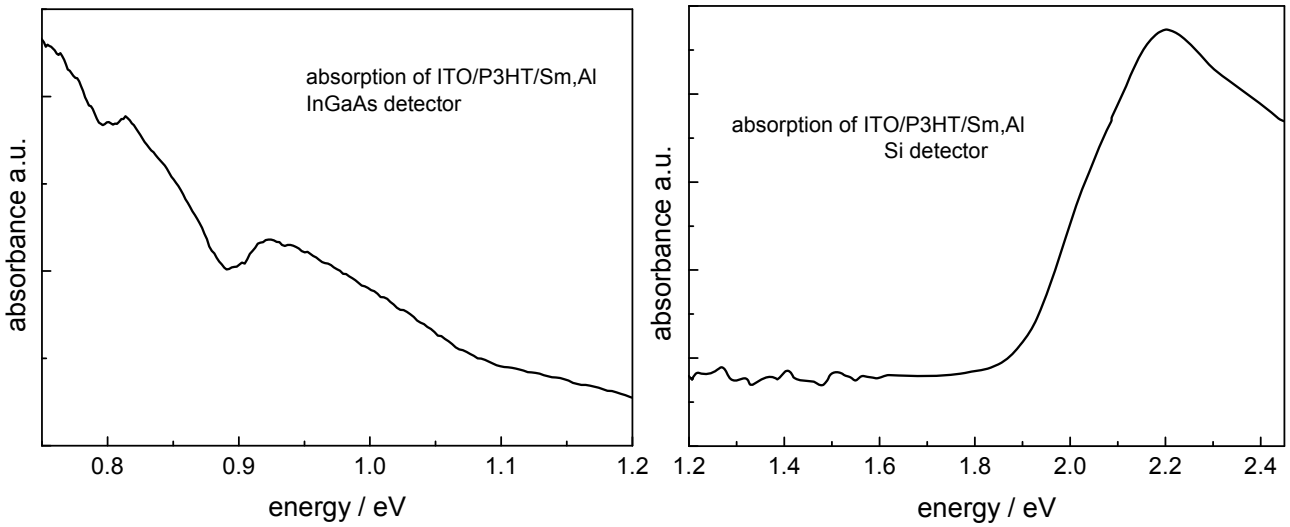

(a) (b)

Figure 4.1: (a) Absorption spectra of P3HT in the visible range and (b) in the near infrared measured using the lock-in technique.

4.2 P3HT diode

A Schottky contact can be found at the interface between a metal and a doped semiconductor. This effect was discovered in 1874 on inorganic semiconductors by Braun [32]. A theoretical explanation for inorganic semiconductors was developed by Walter Schottky and Nevill Francis Mott in 1938 [33]. Schottky diodes differ from P-N junctions in the way that they operate only with a single type of carrier, the majority carriers [34].

Schottky type contacts also appear between metals and slightly doped organic semiconductors like P3HT. Due to the work-function difference between the metal and the semiconductor, a potential-barrier appears. This potential barrier can be reduced by an externally applied voltage, so that charge carriers can pass through, and it prevents significant leakage current flow at the reverse bias, which leads to a diode like behavior. Such diode characteristics are also observed in our samples (figure 4.3). The amount of charge carriers within a diode depends upon the applied bias, the temperature and the amount of doping of the semiconductor.

In figure 4.2 a schematic cross section of a P3HT diode is shown. The spectra below were recorded for a sample, with a P3HT layer thickness of 280 nm, for the electrode 20 nm samarium and 80 nm aluminium were evaporated. Samarium has a work function of 2.7 eV (Sm), while ITO has $4.7 - 4.9$ eV [35].

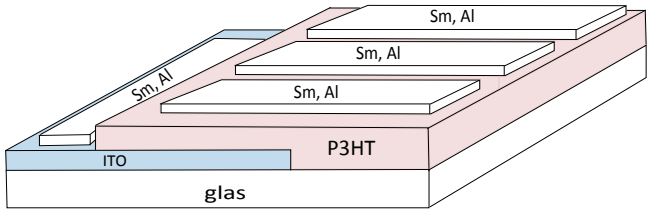

Figure 4.2: Schematic cross section of an P3HT-Diode

A diode characteristic of the device is shown in figure 4.3.

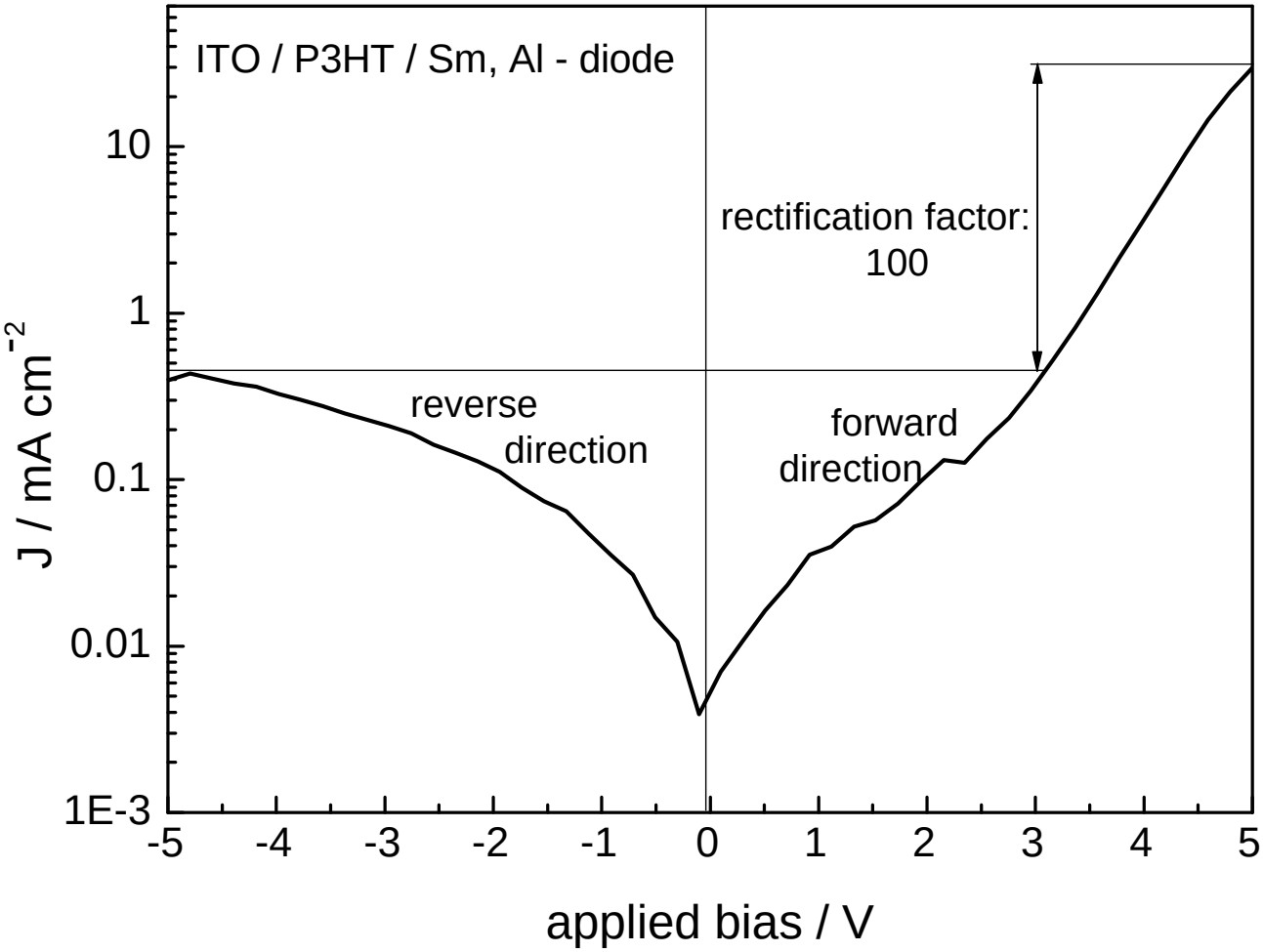

Figure 4.3: Diode-characteristic of a P3HT sample.

The CMS spectra, as shown in figure 4.4, of the P3HT diode where taken in a spectral range between 2.5 and 1.25 eV, which is the visible range of the electromagnetic spectrum.

Operating the diode in reverse bias, the width of the depletion layer is increased, therefore the amount of current is lower, as seen in figure 4.3. In case of reverse bias a strong EA signal is observed (peak at 1.9 eV) at the absorption edge of P3HT (figure 4.1b). In our samples we found the maximum height of the EA signal for -3 V (figure 4.5b), there the CMS signal is, as expected, weak (see chapter 2.3).

Operating the diode in forward bias the width of the depletion layer is lowered, more mobile charge carriers in the polymer are observed. Therefore the EA signal is weak, while the CMS signal is strong and features around 1.7 eV and around 1.3 eV arise, which are, according to literature, the C3 and C3' transitions (figure 2.4).

The CMS signal is at its maximum for 1 V, with further increase of the bias the signal saturates. This weakening of the signal at higher voltages is due to the fact that the lock-in amplifier is only sensitive to the relative changes and not to the absolute charge carrier concentrations.

In comparison to an already high magnitude of charge carriers the amount of injected charge carriers is low, while for a low concentration the change is high.

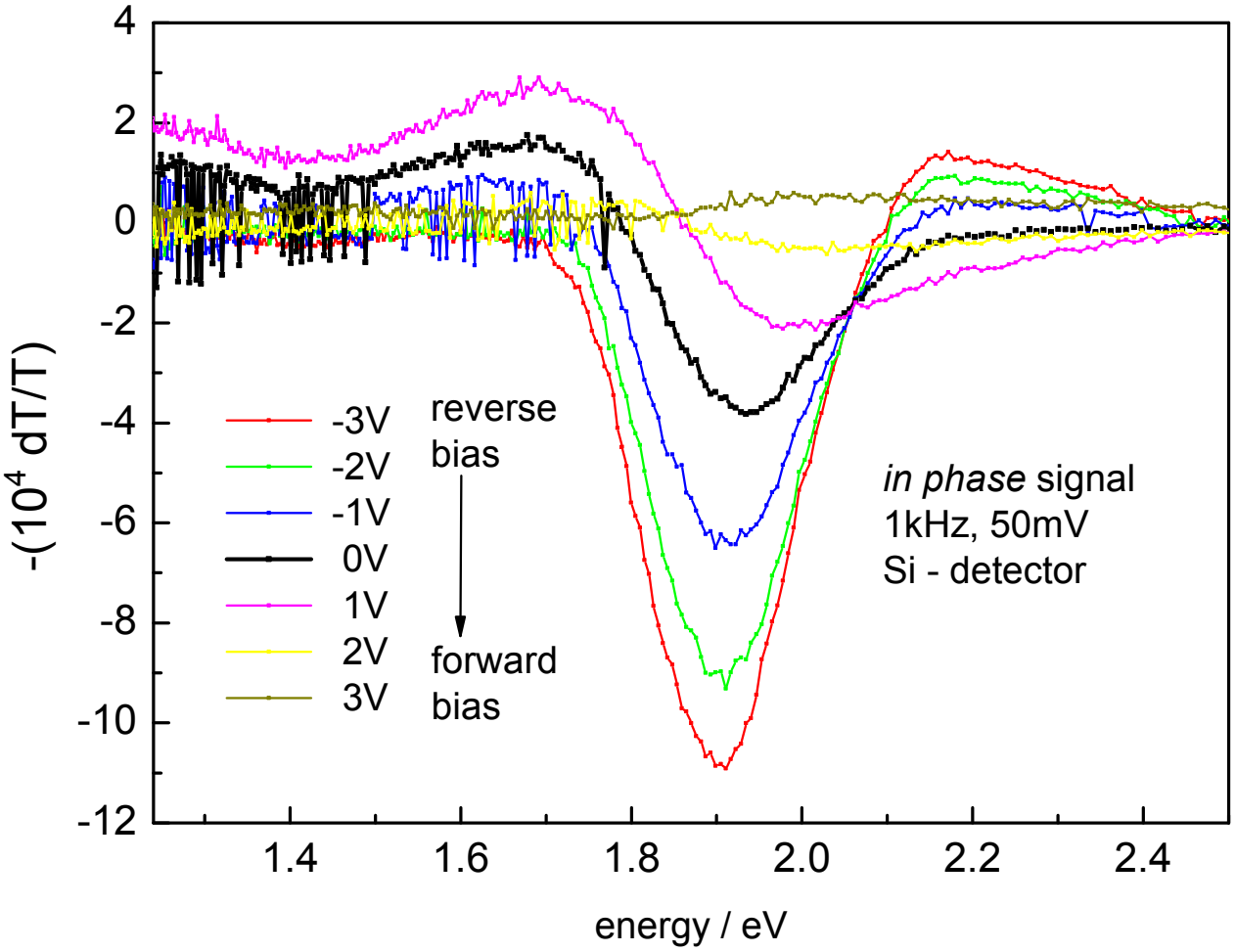

Figure 4.4: EA and CMS spectra of a P3HT diode.

If no bias is applied to the diode the intrinsic charge carriers can be observed (figure 4.5a). For the diode biased in reverse mode we do not observe a CMS signal (figure 4.5b). The small peak just before the EA signal at 2.15 eV (figure 4.5b) is reported earlier in the literature [25]. Biasing the diode towards forward direction the smaller peak at lower wavelengths disappears.

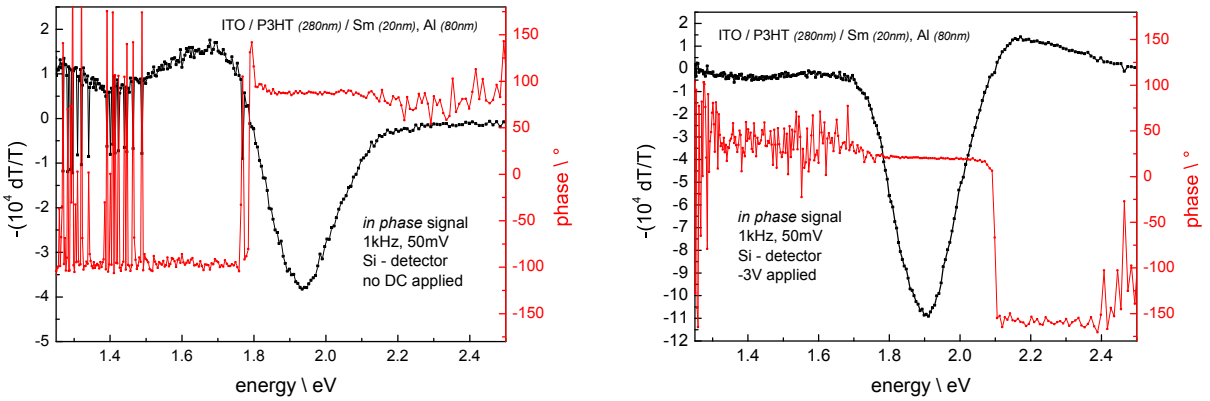

(a) (b)

Figure 4.5: (a) CMS spectra for the P3HT diode taken with no bias applied and (b) CMS spectra for the P3HT diode taken at $-3\,\mathrm{V}$ (reverse bias).

For the diode being biased from depletion towards forward direction the height of the EA peak decreases and finally becomes 0, as the injected charge carriers screen the external field (figure 4.6).

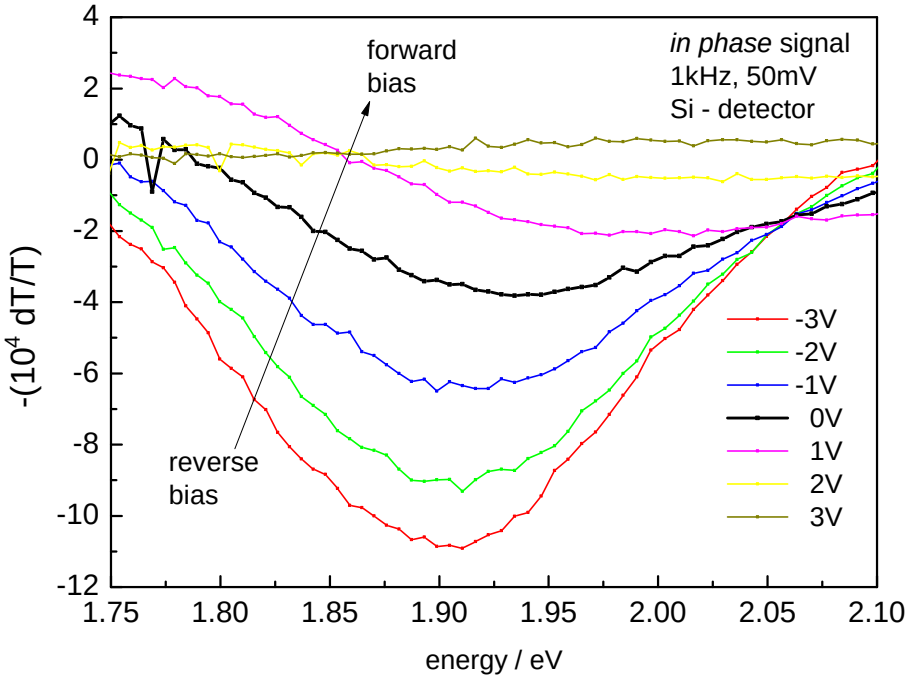

Figure 4.6: EA and CMS spectra of a P3HT diode.

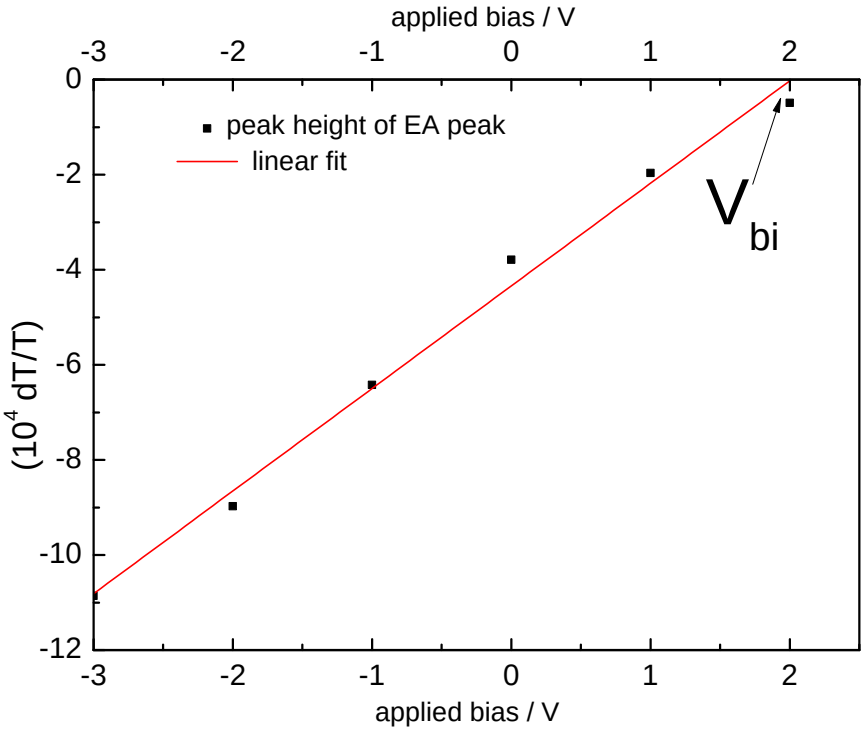

Figure 4.7: Estimation of the built-in potential by a linear fit.

The graph 4.7 shows a linear fit of the $(\frac{-\delta T}{T})$ values of the maximum of the EA signal from -3 to 2 V, which, by extrapolation, leads to an estimation of the built-in field of 2 eV. The built in field can be read out at the intersection of the linear fit with the x-axis.

The position of the maximum of the EA peak changes with the applied DC bias, driving the bias towards forward direction the maximum moves to higher energies (figure 4.6).

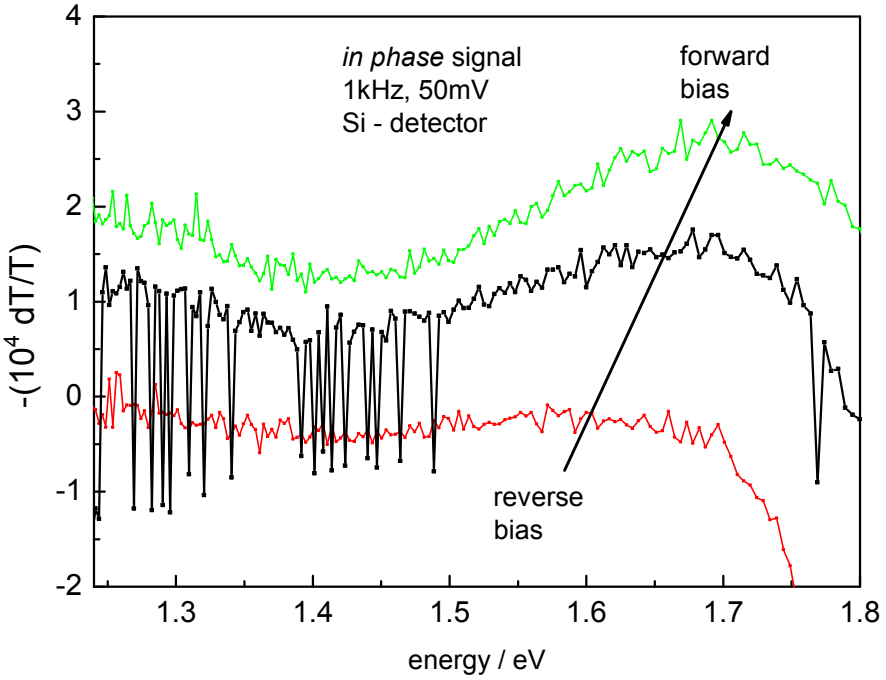

Figure 4.8: Increase in spectral features for biasing the diode in forward direction (−3 V (red), 0 V (black), 1 V (green)).

By applying an increasing positive voltage to the diode spectral features due to the charge carriers are observed (figure 4.8). Two peaks centered around 1.7 eV and 1.25 eV are detected, which is in accordance with measurements by Brown and Sirringhaus [3], who state that the C3' and the C3 peaks occur at 1.35 eV and 1.75 eV.

4.3 MIS devices

A field effect transistor (FET) utilizes a metal-insulator-semiconductor (MIS) structure. The application and modulation of a voltage to the MIS structure causes an interfacial doping.

For MIS structured samples with P3HT as p-type semiconductor and a gold electrode, a negative gate voltage attracts positive charge carriers to the insulator/semiconductor interface to form an accumulation layer (figure 3.7). Superposition of an AC modulation voltage in addition to the DC gate bias results in a modulation of the charge density at the interface. Consequently a positive gate voltage repels positive charges from the interface and a highly insulating depletion layer is formed.

The capacitance of the gate dielectric determines the operating voltage of the device. The surface characteristics of the insulator affect the structure of the semiconductor at the interface [36] [28] [14].

Charges which are trapped at the semiconductor/insulator interface or that leak through the insulator interact with the light but do not change and are therefore not seen as features in the absorption spectra [23].

4.3.1 Interfacial doping on MIS structured samples

Samples with an insulating BCB resin layer were prepared, as shown in figure 4.9.

The spectra presented below where taken from a sample with a layer thickness of BCB of 1 μm and 200 nm of P3HT.

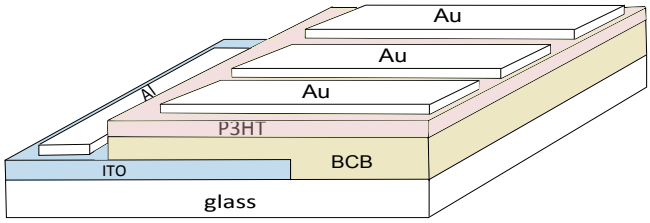

Figure 4.9: Schematic cross section of an MIS structured sample.

Measurements were performed from -200 to $+200$ V, in the visible and the near infrared part of the electromagnetic spectrum.

In accumulation mode CMS signals are observed, as can be seen in figure 4.11b. In the visible range a peak at 1.27 eV and a broad band starting at 1.9 eV with a shoulder at 1.45 eV are observed. The feature 1.27 eV and the one at 1.9 eV are in agreement with results found by Ziemelis et al.[37], who state that these optical transitions can be assigned to optical transitions of singly charged polarons. Also Brown and Sirringhaus state these features, although their results are compared to ours shifted for about 0.1 eV to higher energies [3]. The discovered features can be associated to the charge carriers within the polymer chain. The broad band feature is the bleaching of the $\pi - \pi^*$ absorption, which occurs due to the polaronic states located within the gap. The spectra indicate that polarons in P3HT are not confined to a single chain, but are spread over several, π-stacked chains [14]. The π-stacking of the chains leads to a charge transport between the chains.

The results of the optical measurements are also surface-property dependent, because the texture of the interface can influence the structural, optical and the electronic properties of organic films [38].

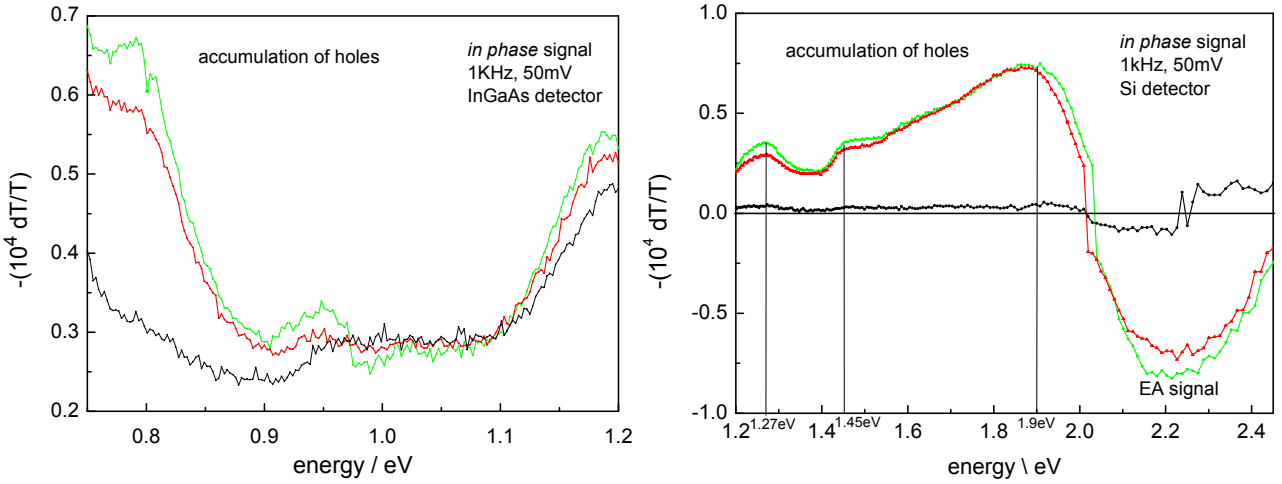

(a) (b)

Figure 4.10: (a) CMS spectra for the BCB-P3HT MIS structured sample biased in the near infrared and (b) CMS spectra for the BCB-P3HT MIS structured sample in the visible, biased at −200 V (green), −100 V (red) and 0 V (black).

In the near infrared, the onset for the peak at 1.27 eV can be seen, as a rise in the signal starting at 0.85 eV (figure 4.11a).

Sirringhaus et al. also state from their CMS measurements that the bleaching, which is a reduction of the strength of the π-π^* absorption ($\frac{-\delta T}{T}$), shows a pronounced vibronic structure, which is more structured and red-shifted compared to the inhomogeneously broadened absorption spectrum of the film [14]. They conclude that the charge carriers move to the most ordered domains in the film. Disorder within the semiconductor film causes the energy of a polaronic charge carrier to vary across the polymer. Defects like the local conformation of the polymer backbone, chemical impurities, structural defects of the backbone result in a broadening of the density of states. Several groups state that the optical and electrical properties of organic semiconducting materials strongly depend on the degree of structural order [39]. This was shown for PPV by the work of Pichler et al. [40]

For the MIS structure in depletion mode the spectra coincide with the one measured at 0 V bias. Therefore it is very likely that electron injection is inhibited due to the device structure (figure 4.11).

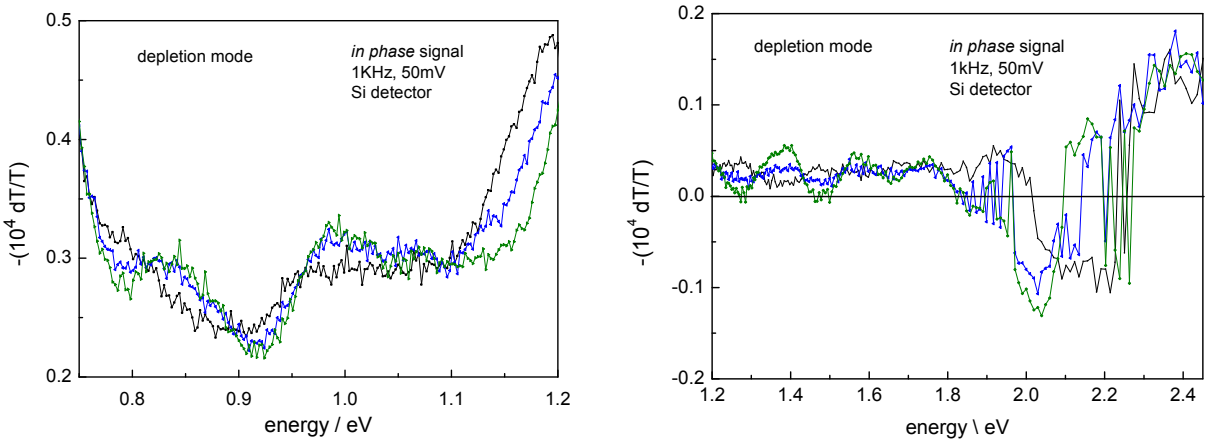

(a) (b)

Figure 4.11: (a) CMS spectra for the BCB-P3HT MIS structured sample in the near infrared and (b) CMS spectra for the BCB-P3HT MIS structured sample in the visible, biased at 200 V (olive), 100 V (blue) and 0 V (black).

Unfortunately it was not possible to overlap the spectra of the visible and the near-IR region, the peaks are of different size. This is a common problem in absorption spectroscopy, which occurs due to the poor sensitivity of the detectors in the overlap region [16].

4.3.2 Electrochemical doping on MIS structured samples

In order to see the effect of chemical doping on the CMS spectra, ion containing dielectrics were used instead of BCB. A schematic of the samples containing $LiClO_4$ as ionic component is shown in figure 4.12. This configuration is basically an electrochemical cell, with the additional PEO + $LiClO_4$ polymer layer as an electrolyte.

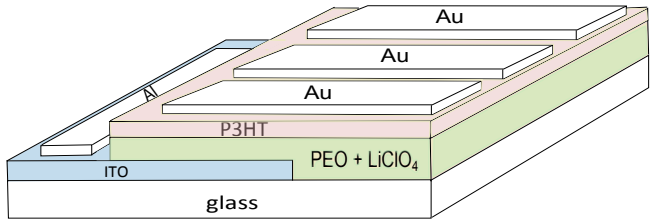

Figure 4.12: Schematic cross section of an MIS structured sample, containing ions.

PEO films were prepared from a 2.5 weight $-$ % solution in acetonitrile, containing 2 mg/ml $LiClO_4$. Film thickness of the layer was measured to be 200 nm. On top of the dielectric, P3HT was spin-coated, so that a film of 250 nm thickness was obtained. For the back electrodes 100 nm of gold were evaporated.

Panzer and Frisbie used in their experiments an ion containing PEO layer as dielectric, to obtain a system with an high relative permitivity ϵ_{eff}, arguing that the ions were immobilised

within the PEO [13]. Such dielectrics show values of about $\epsilon = 1000$ while common dielectrics like BCB have an $\epsilon < 5$.

Gray and Vincent state that $LiClO_4$, dependent upon the concentration, forms complexes with PEO [41]. Nevertheless the PEO layer is a bad insulator as, as Dhoot et al. state, pinholes in PEO are difficult to completely rule out [42]. Therefore chemical doping when using PEO and $LiClO_4$ is very likely. This is also what is seen in our spectra, as those with an ion containing dielectric differ strongly from those with BCB as an insulating layer (figure 4.17).

The form and the position of the charge induced features are very similar in the case of positive and negative voltage applied (figure 4.13a and figure 4.14a), but the intensity grows stronger in the case of negative voltage, while it weakens in the case of positive applied voltage. Spectral intensities are not linked to the absolute charge concentration but to the change in concentration.

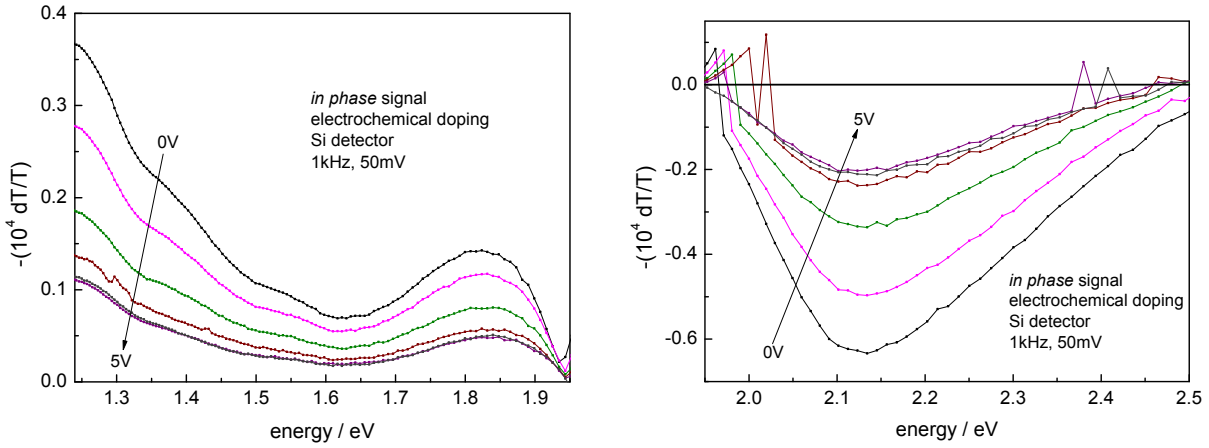

Figure 4.13: CMS spectra of the PEO + $LiClO_4$ - P3HT sample in the visible for 0V to 5V applied, in steps of 1V (a) showing the charge induced features and (b) the EA peak.

As shown in figure 4.13b and figure 4.14b the EA peak is observed around 2.1 eV. On the peakside facing lower energies the peak is more steep than on the other side.

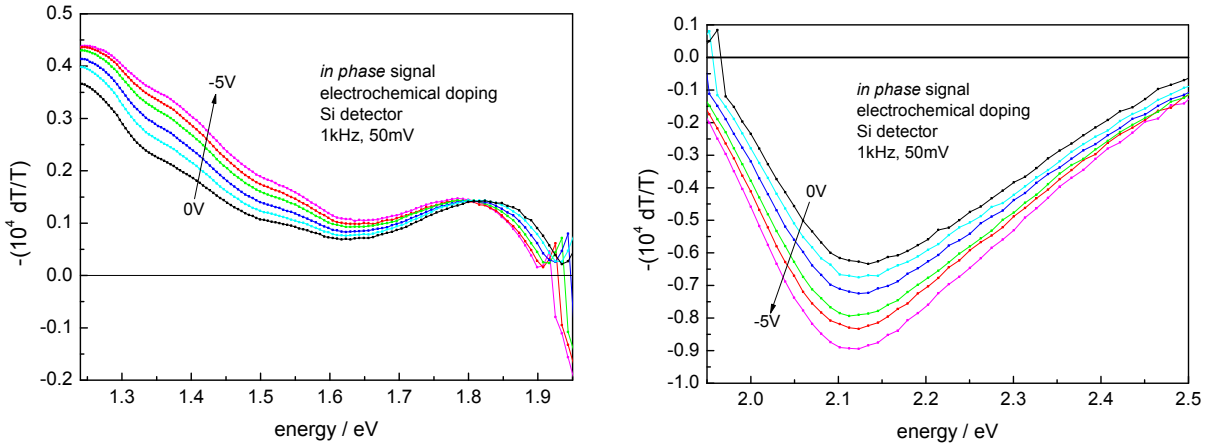

Figure 4.14: CMS spectra of the PEO + $LiClO_4$ - P3HT sample in the visible for 0V to -5V applied, in steps of 1V (a) showing the charge induced features and (b) the EA peak.

Figure 4.15 shows the spectra for the electrochemically doped P3HT in the near infrared. The peak centered at about 1.27 eV is referred to as C3' feature in the literature. There is also a shoulder at 1.05 eV.

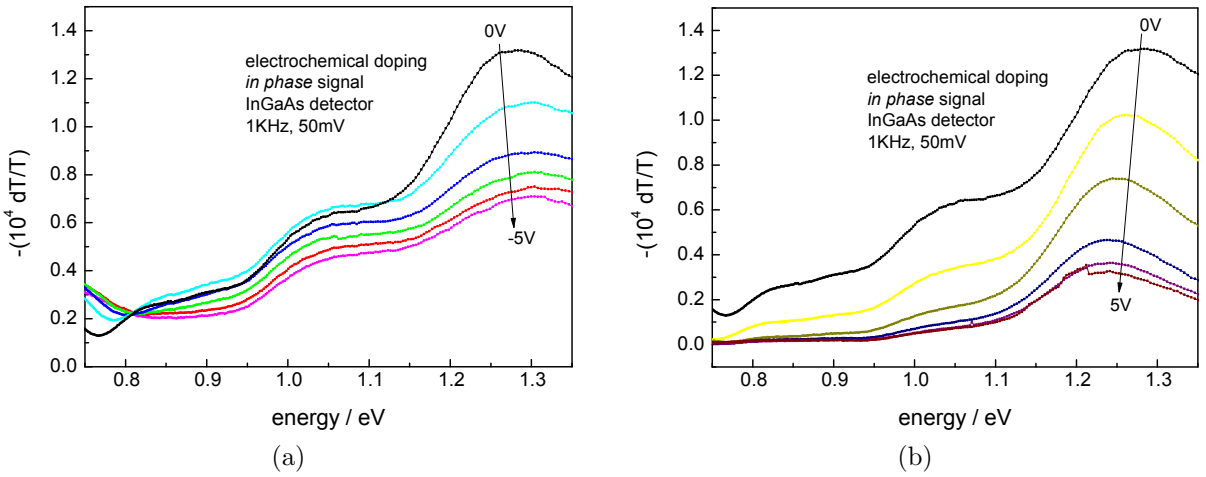

Figure 4.15: (a) CMS spectra for negative bias applied in the near infrared and (b) CMS spectra for positive bias applied in the visible.

For doping in case of an applied bias, the counterions are supplied by the ionic component.

The spectra obtained for negative biases are less intense than those for positive biases (figure 4.16).

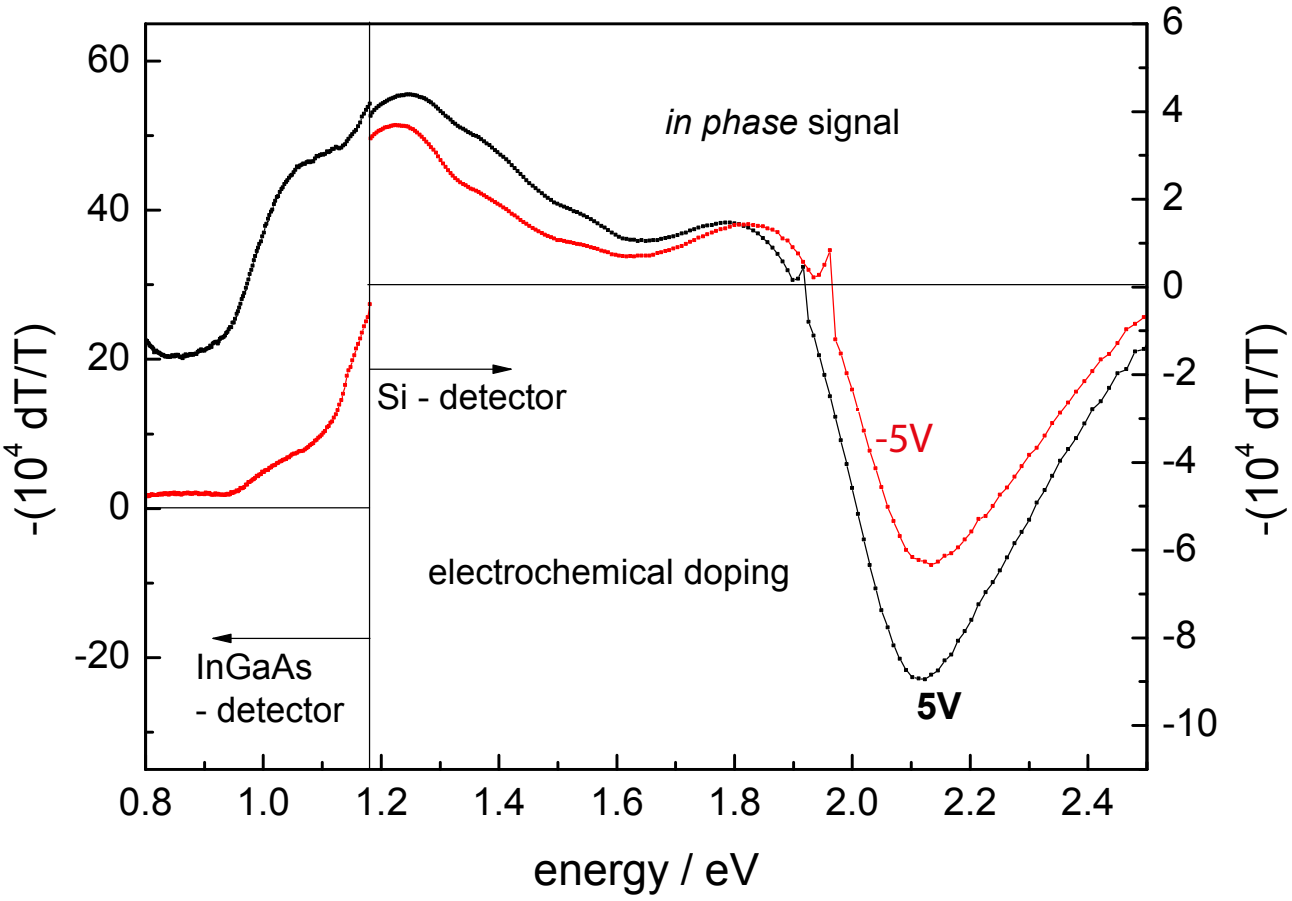

Figure 4.16: Spectra of the PEO + $LiClO_4$ - P3HT sample for −5 V and +5 V applied.

4.3.3 Comparision of interfacial and electrochemical doping

Figure 4.17 shows the comparison of the spectra for the interfacial and for the electrochemically doped P3HT in a MIS structured sample. The EA peak as well as the CMS features is red-shifted compared to the interfacial doped samples. The features change quantitatively which can be attributed to the different kind of doping. Electrochemically doping would effect the bulk P3HT whereas interfacial doping just happens at the interface. This explains, that the very strong feature at 1.9 eV in case of interfacial doping weakens, while the feature at 1.25 eV is increased.

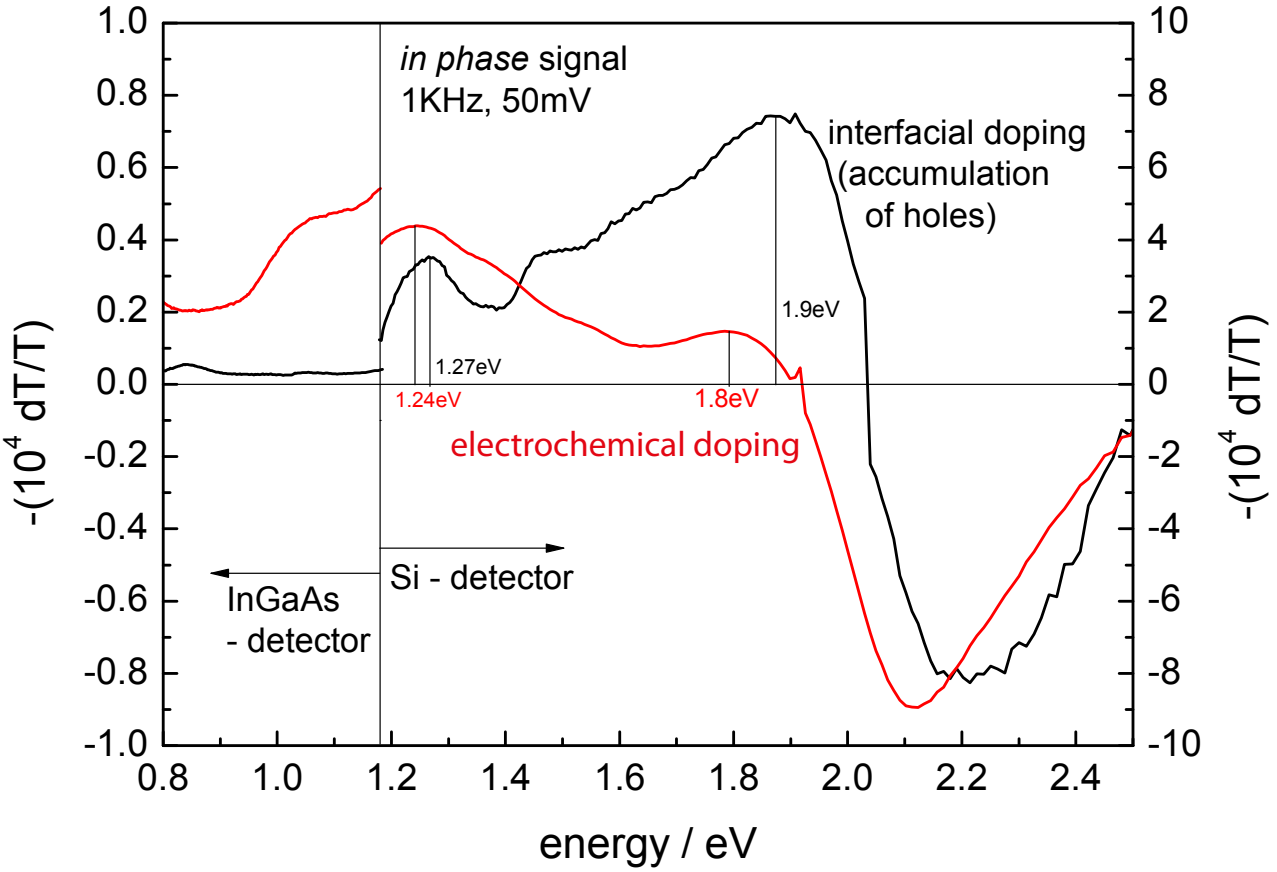

Figure 4.17: Comaprison of the spectra of interfacial doping (black) and electrochemical doping (red).

4.4 ATR-FTIR measurements

Reference measurement

To calibrate the system we measured the blank silicon-gold structure. This reference does not give a signal in the range of interest.

Interfacial doped P3HT

Figure 4.18 shows the schematics of the samples measured with the ATR-FTIR technique. The slightly $p-$doped silicon prism is the ATR crystal, which forms a blocking contact with P3HT within a certain voltage range ($+5\ to\ -5\,\mathrm{V}$), therefore the structure can be seen as a MIS device. Holes can be generated within the interface of the silicon and P3HT where gold acts as the injecting electrode.

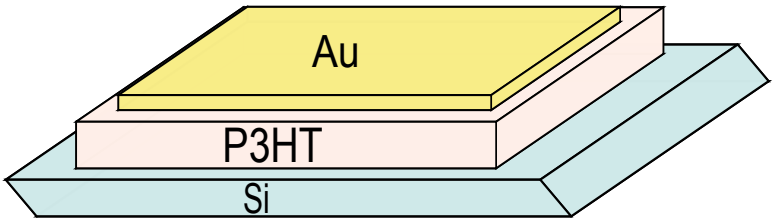

Figure 4.18: Schematic of a FTIR sample.

The P3HT layer was gained by spin-coating, leading to a thickness of 280 nm. On top 80 nm of gold were evaporated.

Difference spectra were calculated from the single beam taken at 5 V and the spectrum taken with no bias applied to silicon, which acts as a gate. A macro was programmed to record 10 scans for every voltage and to repeat this step 1200 times. The voltage was triggered by a relay.

The spectrum is plotted in figure 4.19. Compared to spectroelectrochemical FTIR measurements of Kvarnström et.at [43],[44] we also see similar results. We observe infrared activated vibrational modes (IRAVs) below 0.2 eV (figure 4.20). At 0.2 eV a shoulder of a broad polaronic absorption is seen, which is similar to the findings in the literature cited above.

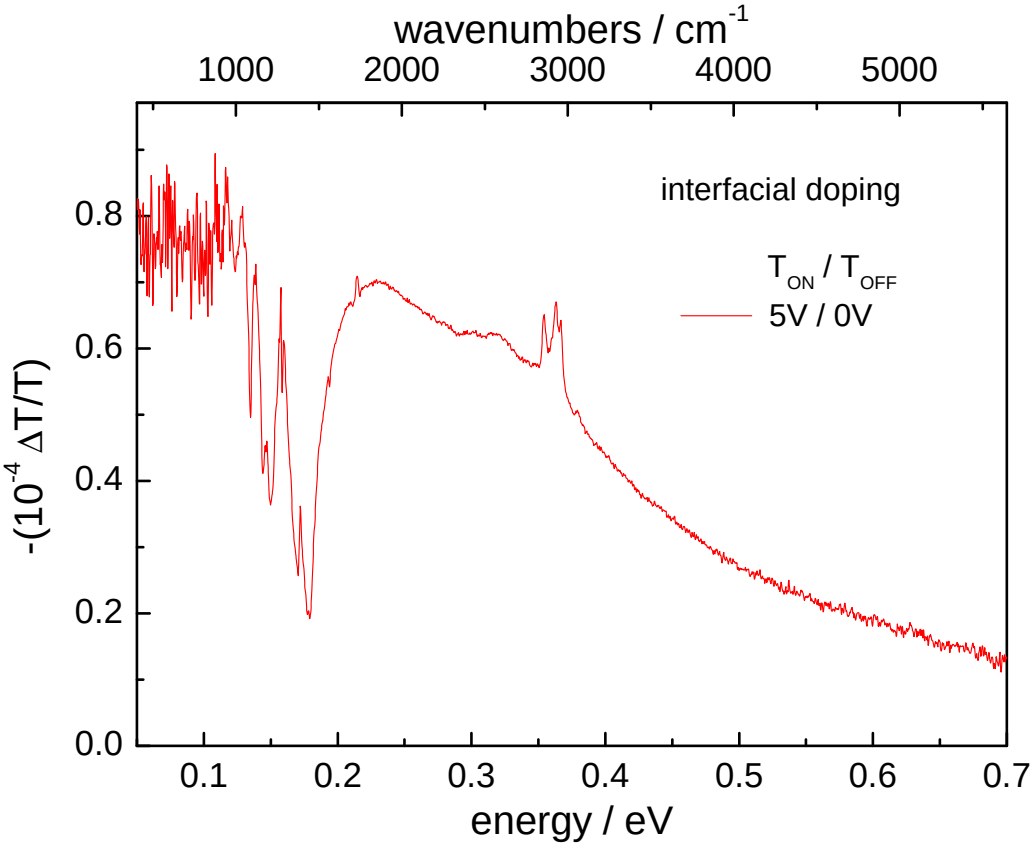

Figure 4.19: CMS - ATR - FTIR difference spectra of a MIS device containing P3HT biased at 5 *and* 0 V

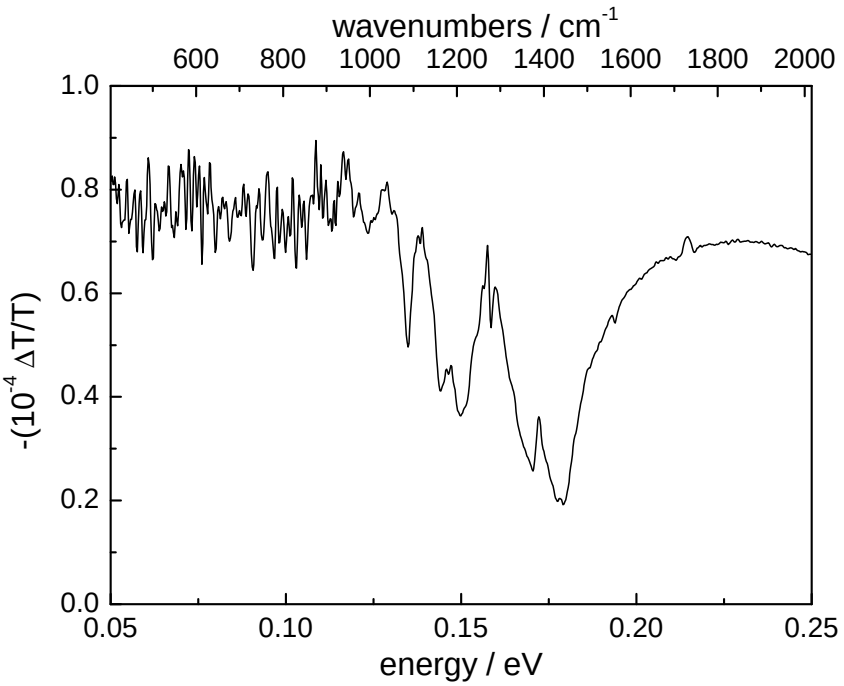

Figure 4.20: IRAV bands of interfacial doped P3HT.

Electrochemically doped P3HT

In order to investigate an electrochemically cell compared to the previous structure shown in figure 4.18 a PEO + $LiClO_4$ layer was inserted between P3HT and gold (figure 4.21). Due to the presence of $LiClO_4$ in PEO a solid state electrolyte, silicon acts as a working electrode while gold on top acts as a counterelectrode. An applied positive voltage leads to p-doping,therefore the polarity is reversed compared to the previous case, where an applied positive voltage caused a depletion of charge carriers (figure 3.8 and 3.7).

In this case we have a reversed polarity

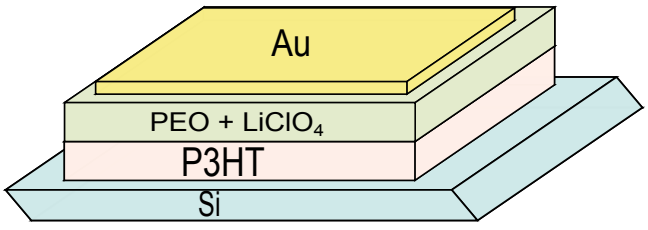

Figure 4.21: Schematic of a FTIR sample with an electrolyte layer.

When a negative bias is applied to the silicon we expect n-doping and p-doping for opposite potentials. The difference spectra were measured in the same way as for the interfacial doping. The sample was biased at the desired polarity (-5 or 5 V and 0 V) for at least 10 s. For every

pulse 10 spectral scans were recorded and this process was repeated 1200 times. As a result differences in the spectra for both cases are observed.

For the FTIR measurements P3HT was spincoated on the silicon-ATR-crystals, on top a gold electrode was evaporated. The thickness of the P3HT-layer was 280 nm. A 2.5 weight − % solution of PEO in acetonitrile, containing 2 mg/ml $LiClO_4$ was used to spincoat the ion containing film.

Spectra are shown in figure 4.22.

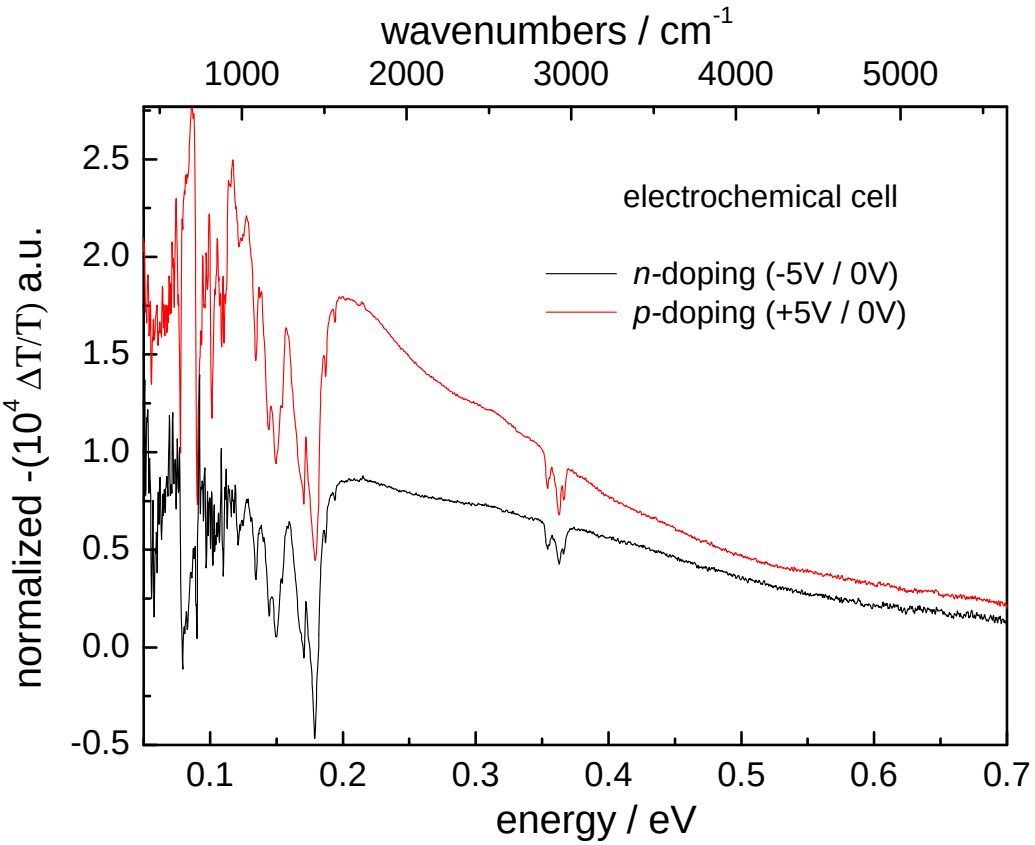

Figure 4.22: CMS - ATR - FTIR difference spectra of a MIS device with P3HT and an additional ion-containing layer, biased at −5 or 5 and 0 V.

For a normalized y-axis the spectral differences, according to the different types of doping, are seen more clearly (figure 4.23).

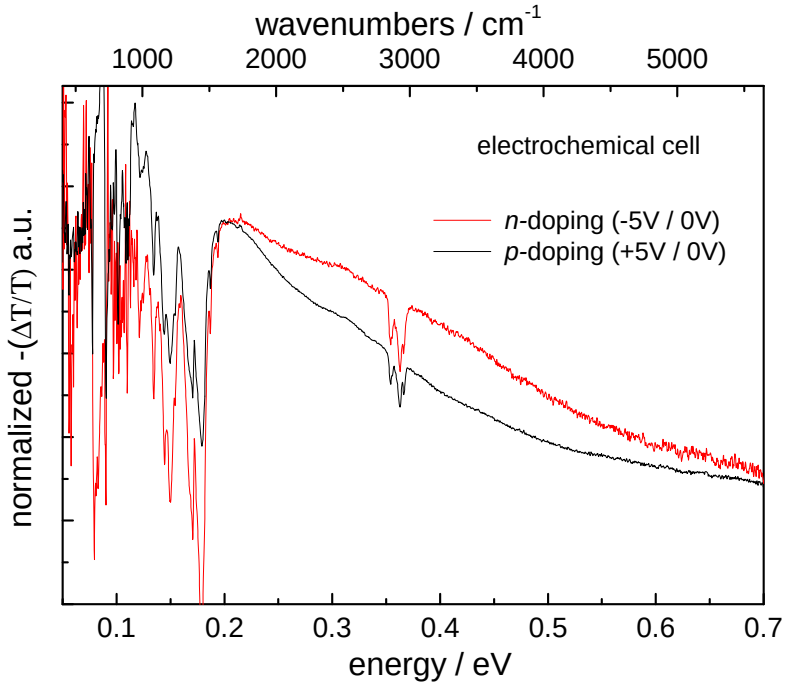

Figure 4.23: Normalized CMS - ATR - FTIR difference spectra of a MIS device containing P3HT and an additional ion-containing layer, biased at −5 or 5 and 0 V.

Comparison

Figure 4.24 shows a comparison of the differential spectra from the interfacial and the electrochemically doped samples, biased at +5 and 0 V.

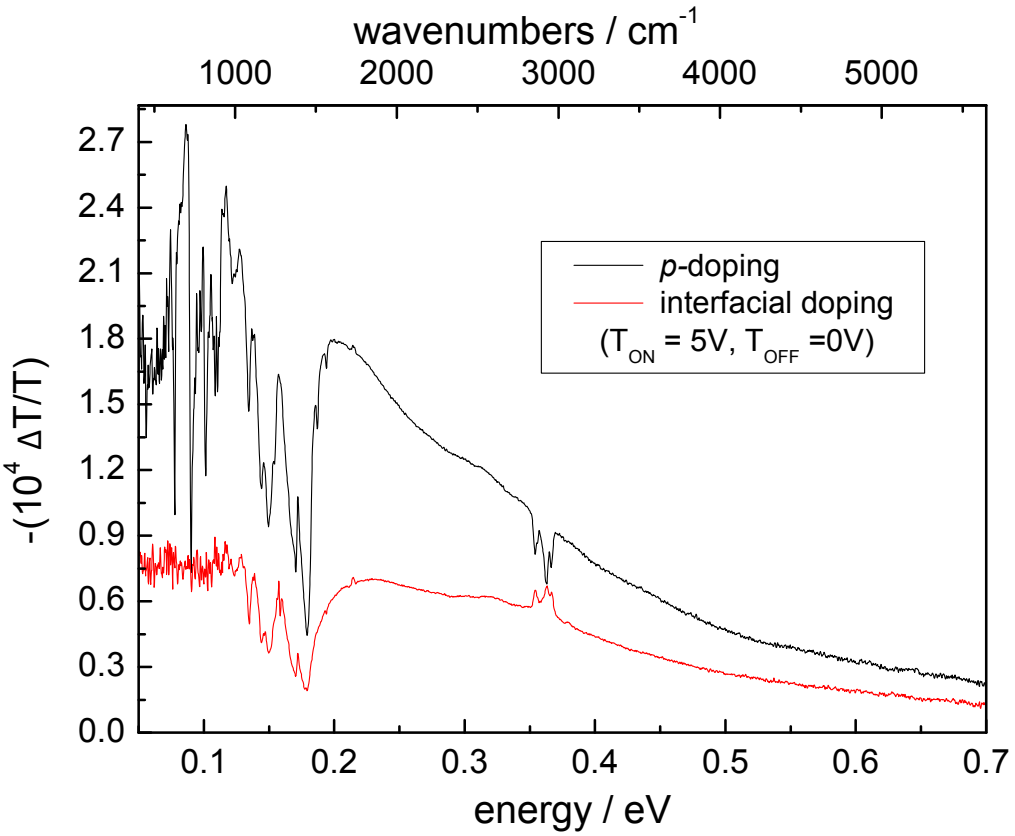

Figure 4.24: CMS - ATR - FTIR difference spectra of devices containing P3HT biased at +5 and 0 V, one containing ions (red) and the other without ions (black).

The IRAV bands show a difference for the different types of doping. For interfacial doping the spectral features are less intense and also the peaks at 0.08 and 0.09 eV, which occur in case of electrochemical doping, are not observed. Although the signals in the spectra for both cases of electrochemical doping are very similar, the features in case of *p*-doping are more distinctive and an additional peak at 0.1 eV is observed (figure 4.25).

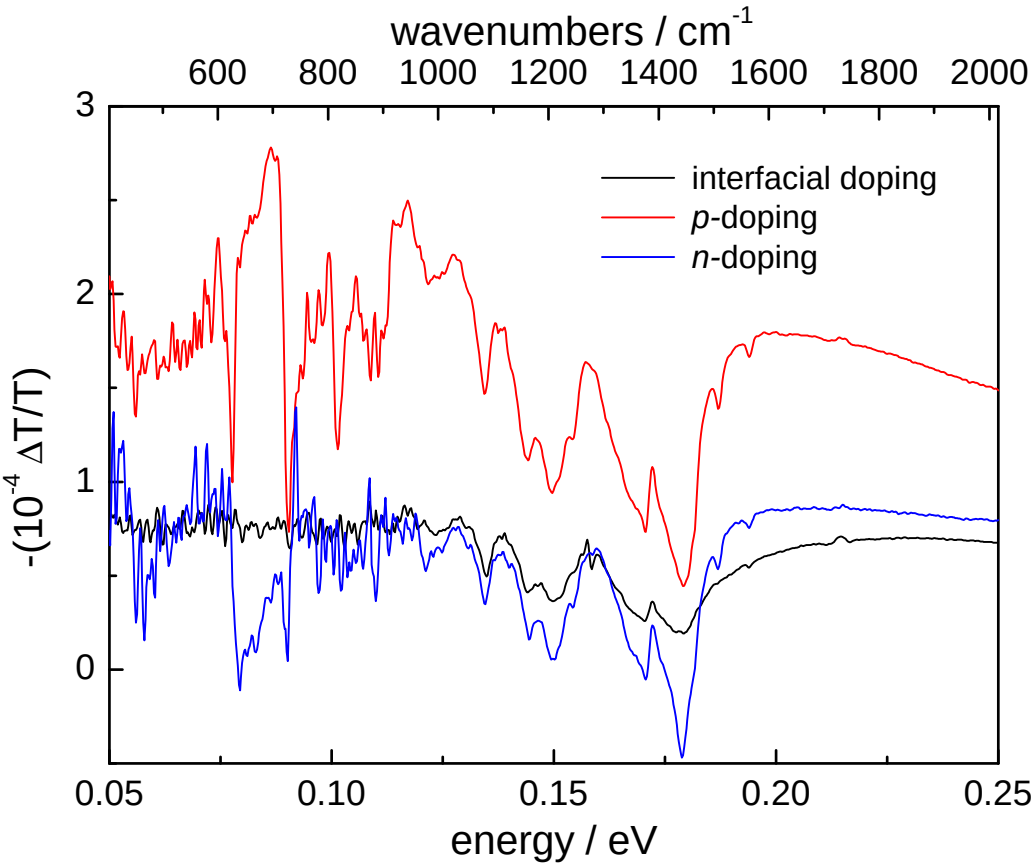

Figure 4.25: IRAV bands of the interfacial (black) and the chemically doped (red and blue) devices.

Two features are observed in the spectra:

- sharp resonances in the $1000-1500\,\mathrm{cm}^{-1}$ range, which result from the IR active vibrational modes (IRAV's)
- a broad polaronic absorption band arising at higher energies than the IRAVs.

This results are in analogy with the results in the diploma thesis of Pinar Frank [45] and the results published by Li et al. [23]. Different IRAV bands indicate a different type of doping. Kvarnström et al. state that the intensity of the IRAV bands increases smoothly with an increasing doping level [43], [44]. Absorptions associated with silicon are spread over a broad frequency range and therefore they have a negligible contribution to the absorption spectra in the mid-IR. [23].

Chapter 5

Conclusion

In this work results are presented using charge modulation spectroscopy for P3HT. CMS is an electooptical method to probe electroabsorption as well as interband transistions, polaronic features and infrared vibration activated bands, from the visible to the mid infrared.

Two methods namely a monochromator and lock-in amplifier technique for the visible and the near infrared and a ATR-FTIR set-up for the mid infrared down to $400\,\mathrm{cm}^{-1}$ were used. This allows a complementary study of P3HT at different interfaces.

To test the setup measurements were started with a simple diode in the visible and the near infrared. As a next step classical MIS structures, using BCB as an insulator, were examined. The results from this measurements are compared to a MIS device using an ion containing PEO layer as dielectric. The spectra show that as soon as ions are involved effects from electrochemical doping arise. This is seen in differences in the charge induced spectroscopic features, which are discussed in this work.

The spectral characterization of charge induced features is an aid to understand the electronic structure within the device under operating conditions.

Chapter 6

Appendix

6.1 list of abbreviations

AC = alternating current

ATR = attenuated total reflectance

BCB = Benzocyclobutene

BLZ =blazing angle

CMS = Charge Modulation Spectroscopy

DC = direct current

EA = Electro Absorption

FTIR = Fourier Transform Infrared Spectroscopy

IRAV = infrared active vibration

MIS = metal insulator semiconductor

OFET = organic field effect transistor

P3HT = Poly(3-hexylthiophene)

PPV = Poly(p-Phenylen-Vinylen)

List of Figures

Bibliography

[1] M. Harrison, D. Fichou, F. Garnier, and A. Yassar, "In situ charge-modulation spectroscopy of oligothiophene field-effect diodes: from sexithiophene towards polythiophene," *Optical Materials*, vol. 9, pp. 53–58, 1998.

[2] P. J. Brown and H. Sirringhaus, "Optical spectroscopy of field-induced charge in self-organized high mobility poly(3-hexylthiophene)," *Physical Review B*, vol. 63, no. 12, pp. 125204–1–11, 2001.

[3] P. J. Brown, H. Sirringhaus, and R. Friend, "Electro-optical characterisation of field effect devices with regioregular poly-hexylthiophene active layers," *Synthetic Metals*, vol. 101, pp. 557–560, 1999.

[4] N. Zhao, Y.-Y. Noh, J.-F. Chang, M. Heeney, I. McCulloch, and H. Sirringhaus, "Polaron localization at interfaces in high-mobility microcrystalline conjugated polymers," *Advanced Materials*, vol. 21, pp. 3759–3763, 2009.

[5] B. Beljonne, J. Cornil, H. Sirringhaus, P. J. Brown, M. Shkunov, R. H. Friend, and J.-L. Brødas, "Optical Signature of Delocalized Polarons in Conjugated Polymers," *Advanced Functional Materials*, vol. 11, no. 3, pp. 229–234, 2001.

[6] E. Itoh, K. Terashima, H. Nagai, and K. Miyairi, "Evaluation of poly(3-hexylthiophene)/ polymeric insulator interface by charge modulation spectroscopy technique," *Thin Solid Films*, vol. 518, pp. 810–813, 2009.

[7] M. L.Chabinyc, "Characterization of semiconducting polymers for thin film transistors," *J. Vac. Sci. Technol. B*, vol. 26, no. 2, pp. 445–457, 2008.

[8] H. Sirringhaus, P. J. Brown, R. H. Friend, M. M. Nielson, K. Bechgaard, B. M. W. Langeveld-Voss, A. J. H. Spiering, R. A. J. Janssen, E. W. Meijer, P. Herwig, and D. M. de Leeuw, "Two-dimensional charge transport in self-organized, high mobility conjugated polymers," *letters to nature*, vol. 401, pp. 685–688, 1999.

[9] E. Itoh, H. Nagai, and K. Miyairi, "Field induced electro-optical characterization in poly-3-hexylthiophene mis capacitor," *Thin Solid Films*, vol. 516, pp. 2568–2572, 2008.

[10] J. Bredas and G. Street, "Polarons, Bipolarons and Solitons in conducting polymers," *Acc.Chem.Res*, vol. 18, no. 10, pp. 309–315, 1985.

[11] T. Prosa, M. Winokur, J. Moulton, P. Smith, and A. Heeger, "Electrical Conductivity in Doped Polyacetylene," *Physical Review Letters*, vol. 39, pp. 1098 – 1101, 1977.

[12] J. A. van Haare, E. E. Havinga, J. L. van Dongen, R. A. Janssen, J. Cornil, and J.-L. Bredas, "Redox states of long oligothiophenes: Two polarons on a single chain," *Chem. Eur. J.*, vol. 4, no. 8, pp. 1509 – 1522, 1998.

[13] Y. Y. Deng and H. Sirringhaus, "Optical absorptions of polyfluorene transistors," *Physical Review B*, vol. 72, pp. 045207– 1–12, 2005.

[14] H. Sirringhaus, "Device physics of solution-processed ofets," *Advanced Materials*, vol. 17, pp. 2411–2425, 2005.

[15] P. Lane, X. Wei, and Z. Vardeny, "Studies of charged excitations in π-conjugated oligomers and polymers by optical modulation," *Physical Review Letters*, vol. 77, no. 8, pp. 1544–1547, 1996.

[16] Y. Deng and H. Sirringhaus, "Optical absorptions of polyfluorene transistors," *Physical Review B*, vol. 72, no. 4, pp. 045207–1–12, 2005.

[17] M. Lehnhardt, S. Hamwi, M. Hopinmg, J. Reinker, T. Riedl, and W. Kowalsky, "Charge carrier densities in chemically doped organic semiconductors verified by two independent techniques," *Applied Physical Letters*, vol. 96, pp. 193301–1 – 193301–3, 2010.

[18] M. Kröger, S. Hamwi, J. Meyer, T. Riedl, W. Kowalsky, and A. Kahn, "P-type doping of organic wide band gap materials by transition metal oxides: A case-study on Molybdenum oxide," *Organic Electronics*, vol. 10, pp. 932–938, 2009.

[19] A. J. Heeger, *Semiconducting and metallic polymers: the fourth generation of polymeric materials*. Nobel Lecture, 2000.

[20] C. Chiang, C. J. Fincher, Y. Park, A. Heeger, H. Shirakawa, E. Louis, S. Gau, and A. G. MacDiarmid, "X-ray Structural Studies of Poly(3-alkylthiophenes): An E xample of an Inverse Comb," *Macromolecules*, vol. 25, pp. 4364 – 4372, 1992.

[21] T. C. Chung, J. H. Kaufman, A. J. Heeger, and F. Wudl, "Charge storage in doped poly(thiophene): optical and electrochemical studies," *Physical Review B*, vol. 30, no. 2, pp. 702 – 710, 1984.

[22] T.-C. Chung, J. Kaufman, A. J. Heeger, and F. Wudl, "Charge storage in doped poly(thiophene): Optical and electrochemical studies," *Physical Review B*, vol. 30, no. 2, pp. 702–710, 1984.

[23] Z. Li, G. Wang, N. Sai, D. Moses, M. M. und M. Di Ventra, A. Heeger, and D. Basov, "Infrared Imaging of the Nanometer-Thick Accumulation Layer in Organic Field-Effekt Transistors," *Nano Letters*, vol. 6, pp. 224–228, 2006.

[24] B. E. A. Saleh and C. Teich, Malvin, *Grundlagen der Photonik*. Wiley - VCH, 2008.

[25] C. Lungenschmied, *Electroabsorption in Organic Diodes*. Linz Institute for Organic Solar Cells, 2004.

[26] Weiser, Gerhard and Horvath, Arpad, *Primary photoexcitations in conjugated polymers: Molecular excitations versus semiconductor band model, chapter 12, Electroabsorption spectroscopy on π-conjugated polymers. Edited by N.S. Sariciftci.* World Scientific, Singapore, 1997.

[27] W. Joseph, P. N.R., S. Suneel, and D. N. Rao, "Electroabsorption Spectroscopy: A versatile tool to measure optical nonlinearities," *Current Science*, vol. 86, no. 9, pp. 1283 –1287, 2004.

[28] D. Burdeaux, P. Townsend, and J. Carr, "Benzocyclobutene (bcb) dielectrics for the fabrication of high density, thin film multichip modules," *Journal of Electronic Materials*, vol. 19, no. 12, pp. 1357–1366, 1990.

[29] C. Kvarnström, A. Ivaska, and H. Neugebauer, "Infrared Spectroelectrochemistry on Conducting Polymers and Fullerenes," *Advanced Functional Molecules and Polymers*, vol. 2, pp. 139–169, 2001.

[30] *Pike Technologies - Spectroscopic Creativity*, Dezember 2010. ATR Crystal Selection, *http://www.piketech.com/technical/crystal-selection-ATR.html* .

[31] M. Hesse, H. Meier, and B. Zeeh, *Spektroskopische Methoden in der organischen Chemie.* Georg Thieme Verlag Stuttgart New York.

[32] N. F. Mott, "Note on the contact between a metal and an insulator or semi-conductor," *Proceedings of the Cambridge Philosophical Society*, vol. 34, pp. 568–572, 1938.

[33] W.Schottky, "Halbleitertheorie der Sperrschicht," *Naturwissenschaften*, vol. 26, p. 843, 1938.

[34] S. Dimitrijev, *Understanding Semiconductor Devices.* Oxford University Press, 2000.

[35] S. Hamwi, J. Meyer, T. Winkler, T. Riedl, and W. Kowalsky, "p-type doping efficiency of MoO_3 in organic hole transport materials," *Applied Physics Letters*, vol. 94, no. 25, pp. 253307–1 – 253307–3, 2009.

[36] H. Klauk, *Organic Electronics - Materials, Manufacturing and Applications.* Wiley - VCH, 2008.

[37] K. Ziemelis, A. Hussain, D. Bradley, and F. R.H., "Optical spectroscopy of field-induced charge in poly(3-hexylthiophene); metal-insulator-semiconductor structures: Evidence for polarons," *Physical Review Letters*, vol. 66, no. 17, pp. 2231–2234, 1991.

[38] T. Kampen, "Electronic structure of organic interfaces - a case study on perylene derivates," *Applied Physics A - Materials Science & Processing*, vol. 82, pp. 457 – 470, 2006.

[39] M. Harrison, R. Friend, F. Garnier, and A. Yassar, "The charged excitations in thin films of α-sexithiophene within semi-transparent field-effect devices: inbvestigation by optical spectroscopy of field-induced charge and by photoimpedance spectroscopy," *Synthetic Metals*, vol. 67, pp. 215 – 221, 1994.

[40] K. Pichler, D. Halliday, D. D. C. Bradley, P. L. Burn, R. Friend, and A. Holmes, "Optical spectroscopy of highly ordered poly(p-phenylene vinylene)," *J.Phys.: Condens. Matter*, vol. 5, pp. 7155–7172, 1993.

[41] F. M. Gray and C. A. Vincent, "Dielectric studies of Poly(ethylene oxide) - based polymer electrolytes using time-domain spectroscopy," *Solid State Ionics*, vol. 28, no. 30, pp. 936 – 940, 1988.

[42] A. S. Dhoot, J. D. Yuen, M. Heeney, I. McCulloch, D. Moses, and A. J. Heeger, "Beyond the metal-insulator transition in polymer electrolyte gated polymer field-effect transistors.," *PNAS*, vol. 103, no. 32, 2006.

[43] C. Kvarnström, H. Neugebauer, A. Ivaska, and N. S. Sariciftci, "Vibrational signatures of electrochemical p- and n- doping of poly(3,4-ethylenedioxythiophene) films: an in situ attenuated total reflection Fourier transform infrared (ATR-FTIR) study," *Journal of Molecular Structure*, vol. 521, pp. 271 –277, 2000.

[44] C. Brabec, H. Johannson, F. Padinger, H. Neugebauer, J. Hummelen, and N. Sariciftci, "Photoinduced FT-IR spectroscopy and CW-photocurrent measurements of conjugated polymers and fullerenes blended into a conventional polymer matrix," *Elsevier, Solar Energy Materials and Solar Cells*, vol. 61, pp. 19–33, 2000.

[45] P. Frank, "Fourier Transform Infrared Spectroscopy of Organic Dielectric / Organic Semiconductor Interface," 2007.